ELEMENTA
Science of the Anthropocene

# Global distribution and trends of tropospheric ozone: An observation-based review

O. R. Cooper[1,2*] • D. D. Parrish[2] • J. Ziemke[3] • N. V. Balashov[4] • M. Cupeiro[5] • I. E. Galbally[6] • S. Gilge[7] • L. Horowitz[8] • N. R. Jensen[9] • J.-F. Lamarque[10] • V. Naik[8,11] • S. J. Oltmans[1,2] • J. Schwab[12] • D. T. Shindell[13] • A. M. Thompson[4,14] • V. Thouret[15] • Y. Wang[16] • R. M. Zbinden[17]

[1]Cooperative Institute for Research in Environmental Sciences, University of Colorado, Boulder, Colorado, United States
[2]NOAA Earth System Research Laboratory, Boulder, Colorado, United States
[3]Morgan State University, Baltimore, Maryland, United States
[4]Department of Meteorology, The Pennsylvania State University, University Park, Pennsylvania, United States
[5]Estación GAW Ushuaia, Servicio Meteorológico Nacional, Tierra del Fuego, Argentina
[6]CSIRO Atmospheric Research, Aspendale, Victoria, Australia
[7]Hohenpeissenberg Meteorological Observatory, German Meteorological Service (DWD), Hohenpeissenberg, Germany
[8]NOAA Geophysical Fluid Dynamics Laboratory, Princeton, New Jersey, United States
[9]European Commission, Joint Research Centre, Institute for Environment and Sustainability, Air and Climate Unit, Ispra, Italy
[10]National Center for Atmospheric Research, Boulder, Colorado, United States
[11]University Corporation for Atmospheric Research, Boulder, Colorado, United States
[12]Atmospheric Sciences Research Center, University at Albany - State University of New York, Albany, New York, United States
[13]NASA Goddard Institute for Space Studies, New York, New York, United States
[14]NASA/Goddard Space Flight Center, Greenbelt, Maryland, United States
[15]CNRS Laboratoire d'Aérologie and Université de Toulouse, Toulouse, France
[16]Ministry of Education Key Laboratory for Earth System Modeling, Center for Earth System Science, Institute for Global Change Studies, Tsinghua University, Beijing, China
[17]CNRM-GAME, Météo-France and CNRS, Toulouse, France

*owen.r.cooper@noaa.gov

## Abstract

Tropospheric ozone plays a major role in Earth's atmospheric chemistry processes and also acts as an air pollutant and greenhouse gas. Due to its short lifetime, and dependence on sunlight and precursor emissions from natural and anthropogenic sources, tropospheric ozone's abundance is highly variable in space and time on seasonal, interannual and decadal time-scales. Recent, and sometimes rapid, changes in observed ozone mixing ratios and ozone precursor emissions inspired us to produce this up-to-date overview of tropospheric ozone's global distribution and trends. Much of the text is a synthesis of in situ and remotely sensed ozone observations reported in the peer-reviewed literature, but we also include some new and extended analyses using well-known and referenced datasets to draw connections between ozone trends and distributions in different regions of the world. In addition, we provide a brief evaluation of the accuracy of rural or remote surface ozone trends calculated by three state-of-the-science chemistry-climate models, the tools used by scientists to fill the gaps in our knowledge of global tropospheric ozone distribution and trends.

**Domain Editor-in-Chief**
Detlev Helmig, University of Colorado Boulder

**Associate Editor**
Paul Palmer, The University of Edinburgh

**Knowledge Domain**
Atmospheric Science

**Article Type**
Review

**Received:** February 27, 2014
**Accepted:** May 16, 2014
**Published:** July 10, 2014

# 1. Introduction

Tropospheric ozone is a short-lived trace gas that either originates naturally in the stratosphere (Junge, 1962; Danielsen, 1968; Stohl et al., 2003) or is produced in situ by photochemical reactions involving sunlight and ozone precursor gases including nitrogen oxides ($NO_x$) and non-methane volatile organic compounds, methane ($CH_4$) or carbon monoxide (The Royal Society, 2008; Monks et al., 2009). These precursors originate from natural sources including wildfires, biogenic hydrocarbon emissions, lightning $NO_x$, and biogenic $NO_x$ emitted from soils, but also from anthropogenic fossil fuel and biofuel combustion, or crop burning. The distribution of anthropogenic ozone precursor emissions around the world generally corresponds to the regions of human habitation with 88% of the population and 90% of fossil fuel $NO_x$ emissions occurring in the Northern Hemisphere (NH). However, emissions from biomass burning, primarily caused by human activity, are roughly equal between the two hemispheres (Dentener et al., 2011). Anthropogenic ozone precursor emission are continually shifting in intensity, declining in Europe and North America while increasing in East Asia (Granier et al., 2011), with a simultaneous shift from NH high latitudes to low latitudes (Parrish et al., 2013).

Initially, the stratosphere was thought to be the primary source of tropospheric ozone (Junge, 1962), however studies in the 1950s revealed that ozone was a component of the Los Angeles smog (Haagen-Smit, 1952) and further research in the 1970s and 1980s concluded that ozone is produced photochemically throughout the troposphere and not just in highly polluted areas such as Los Angeles (Levy, 1972; Chameides and Walker, 1973; Crutzen, 1974; Logan et al., 1981; Liu et al., 1987). Present-day chemical transport and chemistry-climate global models vary in their estimates of the quantity of tropospheric ozone originating from the stratosphere or from in situ photochemistry (Wu et al., 2007), but agree that photochemistry is the dominant source, exceeding the flux from the stratosphere by factors of 7–15 (Young et al., 2013). These same models estimate that approximately 30% of the present-day tropospheric ozone burden is attributable to human activity. With a globally averaged tropospheric lifetime of approximately 23 days (Young et al., 2013), ozone's lifetime is much shorter in the boundary layer where it is more readily destroyed by surface deposition and chemical reactions. Heterogeneity of sources, sinks and lifetime produce a global tropospheric ozone distribution that is highly variable by season, location, and altitude.

At the surface, ozone is an air pollutant that adversely impacts human health, natural vegetation and crop yield and quality (National Research Council, 1991; The Royal Society, 2008; Van Dingenen et al., 2009). Two other critically important roles for tropospheric ozone are as a greenhouse gas with an estimated globally-averaged radiative forcing of $0.40 \pm 0.20$ W $m^{-2}$ (IPCC, 2013), and the primary tropospheric source of the hydroxyl (OH) radical which determines the lifetime of trace gases affected by oxidation.

Due to its importance as a greenhouse gas, and source of OH, current understanding of tropospheric ozone's distribution and trends has been regularly assessed every 5–6 years by the Intergovernmental Panel on Climate Change (IPCC) (IPCC, 2013), and is now assessed annually in the State of the Climate Reports published in the Bulletin of the American Meteorological Society (Blunden and Arndt, 2013). Three of us (Cooper, Ziemke, and Parrish) wrote the tropospheric ozone observation reviews recently published in the Working Group I contribution to the IPCC Fifth Assessment Report (Section 2.2.2.3 Tropospheric Ozone [IPCC, 2013]) and State of the Climate in 2012 (Sidebar 2.1: Tropospheric Ozone [Cooper and Ziemke, 2013]). These reviews provide observation-based assessments of the current understanding of tropospheric ozone distribution and trends, concentrating the findings of the most relevant studies into very short passages of just 1300 words in State of the Climate in 2012 and only 900 words in the IPCC Fifth Assessment Report. A disadvantage of distilling so much information into succinct and accurate summaries, was that a wealth of fascinating material was either omitted, or buried deep in on-line supplementary material.

This review article affords us the opportunity to merge the IPCC and the State of the Climate tropospheric ozone summaries, which had slightly different foci, with the relevant material that was omitted. The goal is to describe tropospheric ozone primarily from an observational point of view. We focus on global or regional scale ozone characteristics and therefore rely primarily on observations from rural (defined as outside of major urban areas) and remote sites (islands, mountaintops or clean continental coastal regions). When possible we report data representative of baseline air masses (those air masses unaffected by local sources of pollution [Dentener et al., 2011]), but also contrast the baseline data with ozone measurements made in rural areas of heavily populated and industrialized regions. While we generally relate the ozone distribution to the scientific community's current understanding of ozone precursor emissions and broad photochemical regimes, we do not focus on attribution of ozone sources, a complicated topic best suited for separate in-depth analyses (e.g., Stevenson et al., 2006; Monks et al., 2009; Lamarque et al., 2010; Dentener et al., 2011; Stevenson et al., 2013; Young et al. 2013). Because so many of the studies discussed in this review were conducted independently, we also include some new and extended analyses using well-known and referenced datasets to draw connections between ozone trends and distributions around the world (the sources of these data are listed in the Appendix). In addition, we provide a brief evaluation of the accuracy of rural or remote surface ozone trends calculated by three state-of-the-science chemistry-climate models, the tools used by scientists

to fill the gaps in our knowledge of global tropospheric ozone. The end result is a more thorough assessment of our current understanding of the distribution and trends of tropospheric ozone.

## 2. Early ozone observations

Ozone was first observed in the 19th century with the reliability and relevance of these data critically assessed by Bojkov (1986), Volz and Kley (1988), Lefohn et al. (1992), Marenco et al. (1994) and Pavelin et al. (1999). As described by Bojkov (1986), Christian F. Schönbein, Professor of Chemistry at Basel, Switzerland, discovered the existence of ozone in 1839. Work by Schönbein and other European scientists over the next 25 years finally determined that ozone was composed of three oxygen atoms. During this period Schönbein developed a semi-quantitative method of measuring the abundance of ozone in the atmosphere using strips of paper coated in a mixture of starch and potassium iodide (KI). These paper strips were incorporated into the Schönbein ozonoscope in which a strip of paper was exposed to air, allowing ozone in the air to react with the potassium iodide, which turned the paper a shade of blue. After a 12-hour exposure the color of the paper was compared to a 10-grade chromatic scale that indicated the relative amount of ozone in the air; this value corresponded to the maximum ozone concentration during the 12-hour period. The accuracy of this technique was hampered by dependence of the results on humidity, air flow, other oxidants present in the air and accidental exposure to sunlight. Despite the limitations of this method, beginning in the 1850s, over 300 sites were established around the world to measure ambient ozone. A major reason for the interest in ozone at that time was the erroneous belief that ozone could reduce the spread of epidemics (Bojkov, 1986).

The only quantitative measurements of ozone during the 19th century were made at the Paris Municipal Observatory in Park Montsouris, which was located on the outskirts of Paris. From 1876 until 1907 under the supervision of Chief Chemist Albert-Lévy, ozone was measured by bubbling a known quantity of air through an aqueous solution of iodide ($I^-$) and arsenite ($AsO_3^{3-}$). In the first step ambient ozone oxidized $I^-$ to $I_2$, and in the second step $I_2$ reacted with $AsO_3^{3-}$, forming back $I^-$ and $AsO_4^{3-}$ (arsenate). By titrating the residual arsenite in an alkaline medium with a volumetric standard solution of iodine, one could calculate the quantity of ozone in the air. Volz and Kley (1988) conducted a reanalysis of the Montsouris data by reconstructing Albert-Lévy's Montsouris ozone instrument; they found that this early technique produced results similar to a modern ultraviolet absorption instrument. Volz and Kley determined that ozone was greater when winds were from the rural sector to the southwest, compared to when winds were from the polluted Paris urban area to the northeast. They found that $SO_2$ emissions in Paris likely interfered with the measurement technique and therefore applied a correction to the observed mixing ratios that increased linearly from 2 ppbv in 1881 to 5 ppbv in 1905. They concluded that average ozone mixing ratios at Montsouris during 1876–1910 were 11 ppbv with an uncertainty of ± 2 ppbv due to the $SO_2$ correction. While these measurements indicate that late 19th century ozone in western Europe was much lower than today, there is no way to know if these values were representative of other surface locations in the NH.

In contrast to the quantitative Montsouris ozone measurements, the Schönbein method could only indicate the relative quantity of ozone. During the 1980s and 1990s several researchers admirably attempted to convert late 19th century and early 20th century Schönbein measurements to ozone mixing ratios using a regression between the quantitative Montsouris measurements and coincident Schönbein measurements (Bojkov, 1986) and/or relationships between modern ultraviolet absorption ozone measurements and reconstructed Schönbein papers (Linvill et al., 1980). A major limitation of these approaches is the confounding non-linear sensitivity of Schönbein papers to relative humidity (Linvill et al., 1980). For example, Bojkov (1986) found that Schönbein measurements in the late 19th century erroneously indicated greater ozone at night than during the day due to biases caused by humidity. Another major limitation is the inconsistency between the methodology at Montsouris and other stations around the world, with varying chromatic scales and formulations of Schönbein papers being the most prominent. Following is an illustration of the problems associated with reconstructing ozone mixing ratios from the late 19th century. Linvill et al. (1980), using their humidity corrected empirical relationships between modern ultraviolet absorption ozone measurements and reconstructed Schönbein papers, determined that average daytime ozone at Lansing, Michigan for all months during 1876–1880 was 35 ppbv. Bojkov (1986) applied his derived Montsouris regression to measurements from eleven Schönbein ozonoscopes across Michigan, and found lower ozone values compared to the method of Linvill et al. (1980). Several years later Bojkov's analysis was shown to be incorrect by Marenco et al. (1994) who demonstrated that an error in Bojkov's regression equation led to ozone estimates that were too high by a factor of three, further increasing the discrepancy between the Linvill et al. and Bojkov reconstructions.

Revisions to Bojkov's method as well as application of Linvill et al.'s method have produced late 19th century and early 20th century ozone mixing ratio estimates for Moncalieri in northern Italy (1868–1893) (Anfossi et al., 1991); Montevideo, Uruguay (1883–1885) and Cordoba, Argentina (1886–1892) (Sandroni et al. 1992); Athens, Greece (1901–1940) (Cartalis and Varotsos, 1994); five Southern Hemisphere (SH) and seven NH sites with varying time series between 1872 and 1928 (Pavelin et al., 1999); Malta in the Mediterranean Sea (Nolle et al., 2005); and Zagreb, Croatia (1889–1900) (Lisac et al., 2010). Due to the uncertainty in the

absolute ozone mixing ratios derived from Schönbein measurements (Marenco et al., 1994; Pavelin et al., 1999; Staehelin and Schnadt Poberaj, 2008), those values are not summarized here. However a review of the studies listed above reveals two general conclusions: 1) whether the Schönbein measurements occurred in rural or urban areas, the northern or southern hemisphere, 19th century seasonal ozone most often peaked in spring, followed by winter, with some spring peaks continuing into early summer; seasonal ozone minima most frequently occurred in summer and autumn, although winter minima were not unusual; 2) studies that compared late 19th century estimated ozone mixing ratios to late 20th century ultraviolet absorption ozone measurements generally concluded that ozone increased by about a factor of two during the 20th century.

Despite the uncertainty of the Schönbein method, there is one set of late 19th century Schönbein measurements converted to mixing ratios that is difficult to dismiss. Measurements made between 1874 and 1909 at Pic du Midi, France, 3000 m above sea level, used the same type of paper and techniques as those employed at Montsouris (Marenco et al., 1994). Accounting for differences in pressure and humidity between Pic du Midi and Montsouris, Marenco et al. used the Montsouris regression to estimate that Pic du Midi ozone mixing ratios were approximately 10 ppbv during 1874–1895, with a springtime peak and wintertime minimum. From 1895 until the end of the record in 1909 ozone increased steadily to 14 ppbv, while ozone at Montsouris at this time decreased. Marenco et al. point out that the increase in ozone at Pic du Midi coincided with global increases in methane concentrations, while the ozone decrease at Montsouris may have been the result of increased emission of NO in Paris that destroyed ozone at nearby Montsouris. These time series are the only known records that provide reliable quantitative or semi-quantitative insight into the changing photochemical environment over Europe in the early 20th century. While the Pic du Midi ozone mixing ratios appear to be more reliable than any other record outside of Montsouris, the results raise the obvious question of why ozone at 3 km above sea level at Pic du Midi, a site heavily influenced by the free troposphere, was no greater than ozone at the low elevation site of Montsouris. This lack of a vertical ozone gradient in the lower troposphere is in direct contrast with ozonesonde observations from around the world that showed a consistent increase in ozone with altitude during the 1980s and 1990s (Logan, 1999). The latest generation of atmospheric chemistry models taking part in the Atmospheric Chemistry and Climate Model Intercomparison Project (ACCMIP) show a vertical ozone gradient in the northern mid-latitude lower troposphere during the 1850s that is weaker than the period 1996–2005, but the models overestimate 1850s lower tropospheric ozone by a factor of two (compared to Pic du Midi and Montsouris) (Stevenson et al., 2013). Due to the uncertainty of lower tropospheric ozone predicted by models for the 1850s, there is presently no explanation for the observed lack of an ozone vertical gradient above France in the late 1800s.

## 3. Ozone trends

By the 1930s ozone measurements by the Schönbein technique were no longer made at most locations and reliable quantitative methods were more commonly employed. Marenco et al. (1994) show in their Figure 5 an exponential increase in ozone across western Europe using measurements from several locations, beginning with the Pic du Midi Schönbein measurements in the 1870s followed by short-term quantitative measurements at several high altitude sites in Switzerland, Germany, and France from the 1930s through the early 1990s. Those authors concluded that ozone increased by a factor of 5 between the late 1800s and the early 1990s and by a factor of 2 between the 1950s and early 1990s. This increase corresponds to the global increase in fossil fuel combustion recently summarized by the IPCC Fifth Assessment Report (see figure TS.4 in IPCC [2013]). Similar conclusions were drawn by Staehelin et al. (1994) using additional data sets from the 1930s–1950s in central Europe. They found that ozone in the alpine valley surrounding Arosa, Switzerland increased by a factor of 2.2 from the 1950s to 1989–1991. Analysis of other sites in central Europe showed that ozone increased with similar rates at several elevations between sea level and 3.5 km from the 1930s/1950s until 1988–1991. These ozone increases coincided with rising European $NO_x$ emissions that increased by a factor of 4.5 between 1955 and 1985 (Staehelin et al., 1994).

The world's longest continuous ozone record is from the Arkona-Zingst site on the northern German coast (Feister and Warmbt, 1987; Parrish et al., 2012). Measurements began at Cape Arkona in 1956 using a wet chemical method until 1990 (Warmbt, 1964), after which continuous ozone measurements began at the nearby coastal site of Zingst, 60 km to the southwest. Combining the two sites produces a continuous record with more than 57 years of data (Figure 1). In the late 1950s and early 1960s yearly average ozone values were in the 15–20 ppbv range, which doubled by the end of the 20th century, in agreement with the high elevation European ozone trends compiled by Marenco et al. (1994) and Staehelin et al. (1994).

Spurred by the goals of the International Geophysical Year (IGY) to expand geophysical observations globally, exploratory ozone measurements were made at remote sites in Antarctica (Wexler, 1960) and Mauna Loa, Hawaii in 1957–1958 (Junge, 1962). Comparison of the 1957–1958 measurements from the sea-level site of Little America on the Ross Ice Shelf (based on a 12-month running mean from April 1957 until October 1958) to the same time period at Arkona on the northern German coast shows that annual average ozone was greater at Little America, 22 ppbv vs. 14 ppbv, respectively. However, the greater values at

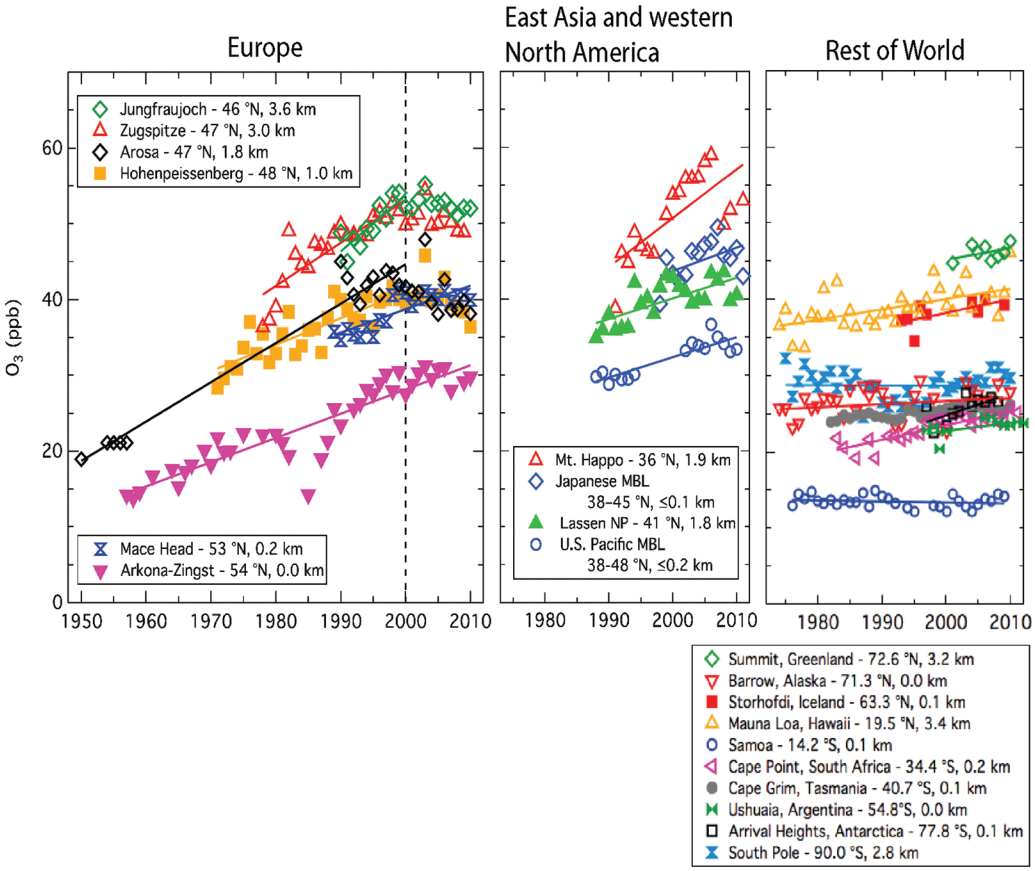


**Figure 1**

**Surface ozone time series at several rural sites around the world.**

Trend lines are fit through the yearly average ozone values using the linear least-square regression method. Trend lines in Europe only extend through 2000 when the positive trend appears to have ended. This figure is modified from the original that appeared in IPCC (2013).

doi: 10.12952/journal.elementa.000029.f001

Little America were driven by enhanced ozone values during the dark winter months. During summertime ozone at Little America was only 14 ppbv while ozone at Arkona was 30% greater (18 ppbv). Comparison of short-term ozone measurements at other coastal Antarctic sites to Arkona in the early and mid-1960s yields similar results (Oltmans and Komhyr, 1976).

In the 1970s quantitative ozone measurements became more widespread and efforts were made to routinely monitor the atmosphere at rural and remote locations for the purposes of detecting long-term changes in the global composition of the atmosphere (Figure 1 and Table 1). Continuous records in southern Germany began at the rural hilltop site of Hohenpeissenberg in 1971 and the mountaintop site of Zugspitze (2670 m) in 1978 (Gilge et al., 2010), while continuous measurements began at the summit of Whiteface Mountain in upstate New York in 1973 (Oltmans et al., 2013). Ozone measurements at remote sites were established by the U.S. National Oceanic and Atmospheric Administration at its baseline observatories of Mauna Loa, Hawaii (1973), Barrow, Alaska (1973), the South Pole (1975), and American Samoa (1976) (Oltmans et al., 2013). Routine ozonesonde profiles became available in Germany, the US, Japan and Antarctica in the early 1970s (Oltmans et al., 2013), while ship-borne monitoring of the marine boundary layer of the North and South Atlantic Oceans began in the late 1970s (Lelieveld et al., 2004).

Numerous long term ozone monitoring sites, measuring surface and free tropospheric ozone, were established in the 1980s and 1990s, with some of the most important rural or remote sites being Cape Grim, Tasmania (1982), Cape Point, South Africa (1983), Mace Head, Ireland (1987), Lassen Volcanic National Park, California (1987), Bermuda (1988) and Izaña, Canary Islands (1988). In addition, major regional ozone monitoring networks were established across Europe and North America. While there are many regions of the world still without ozone monitoring, the amount of data now available for ozone trend analysis is relatively extensive, and too cumbersome to briefly summarize with text or even with tables. In an attempt to easily and clearly relay information on ozone trends at multiple sites, Cooper et al. (2012) developed a map-based view of regional ozone trends across the United States. This approach was employed for summarizing global ozone trends in IPCC's Fifth Assessment Report (IPCC, 2013). While very useful for understanding global ozone trends, the IPCC figures are tucked away in an electronic supplement and not highly visible (Hartmann et al., 2013). This review provides updated versions of the IPCC ozone trend plots, including recently published trends from South Korea, South Africa, Argentina, and two additional sites in Europe.

Figure 2 shows all available ozone trends at the surface or within the lowermost troposphere (ozonesondes or commercial aircraft) for three multi-decadal periods: 1950–1979 through 2000–2010, 1980–1989 through

**Table 1. Linear regression results for decadal trends of ozone mixing ratios derived from the yearly mean data shown in Figure 1.** Statistically significant trends are highlighted in bold font. Note that the for the high elevation European sites, trends are only calculated through the year 2000 after which ozone ceased increasing. $\chi_v$ is the root mean square deviation from the straight line fit through the data.

| Site/data set | Years | Slope and 95% confidence limit, ppbv yr$^{-1}$ | y-intercept at year 2000, ppbv | r | $\chi_v$ ppbv |
|---|---|---|---|---|---|
| Summit, Greenland | 2001–2010 | 0.15 ± 0.32 | 45.2 ± 2.2 | 0.41 | 1.0 |
| Barrow, Alaska | 1974–2010 | 0.04 ± 0.06 | 26.7 ± 0.7 | 0.25 | 1.8 |
| Storhofdi, Iceland | 1993–2009 | 0.18 ± 0.19 | 38.2 ± 1.1 | 0.66 | 1.3 |
| Arkona-Zingst, Germany | 1957–2010 | **0.32 ± 0.05** | 28.1 ± 1.0 | 0.92 | 2.3 |
| Mace Head, Ireland | 1989–2010 | **0.31 ± 0.10** | 38.7 ± 0.6 | 0.83 | 1.4 |
| Hohenpeissenberg, Germany | 1971–2000 | **0.35 ± 0.09** | 41.1 ± 1.5 | 0.84 | 2.0 |
| Zugspitze, Germany | 1978–2000 | **0.57 ± 0.16** | 53.2 ± 2.0 | 0.86 | 2.4 |
| Arosa, Switzerland | 1950–2000 | **0.52 ± 0.06** | 44.7 ± 1.6 | 0.98 | 2.1 |
| Jungfraujoch, Switzerland | 1990–2000 | **0.74 ± 0.35** | 53.7 ± 2.1 | 0.85 | 1.6 |
| Lassen NP, California, U.S. | 1988–2010 | **0.27 ± 0.13** | 40.1 ± 0.9 | 0.69 | 2.0 |
| U.S. Pacific MBL | 1988–2010 | **0.27 ± 0.08** | 32.3 ± 0.6 | 0.88 | 1.2 |
| Mt. Happo, Japan | 1991–2011 | **0.65 ± 0.32** | 50.7 ± 1.9 | 0.74 | 3.8 |
| Japanese MBL | 1998–2011 | 0.31 ± 0.34 | 43.7 ± 2.0 | 0.50 | 2.3 |
| Mauna Loa, Hawaii, U.S. | 1974–2010 | **0.14 ± 0.07** | 40.1 ± 0.9 | 0.58 | 2.1 |
| Cape Matatula, Samoa | 1976–2009 | –0.01 ± 0.03 | 13.4 ± 0.4 | –0.18 | 0.73 |
| Cape Point, South Africa | 1983–2011 | **0.19 ± 0.05** | 23.5 ± 0.4 | 0.85 | 0.98 |
| Cape Grim, Australia | 1982–2010 | **0.06 ± 0.02** | 25.3 ± 0.2 | 0.71 | 0.49 |
| Ushuaia, Argentina | 1997–2013 | 0.10 ± 0.11 | 22.8 ± 0.8 | 0.56 | 0.91 |
| Arrival Heights, Antarctica | 1997–2008 | **0.29 ± 0.24** | 24.8 ± 1.1 | 0.67 | 1.2 |
| South Pole, Antarctica | 1975–2010 | –0.00 ± 0.06 | 28.7 ± 0.8 | –0.004 | 1.9 |

doi:10.12952/journal.elementa.000029.t001

2000–2010, and 1990–1999 through 2000–2010. All trend values are from the peer-reviewed literature, or are updates to trends initially reported in the peer-reviewed literature, using the original methods. The trends are based on at least 10 years of data and use yearly average ozone values. The vector-based plotting method indicates the approximate rate of change and statistical significance. The reader should keep in mind that the rate of change is not necessarily constant, for example several sites in Europe showed a strong ozone increase prior to 2000, but no positive trend since (Figure 1). Exact values for the ozone rate of change, and the 95% confidence limits are reported in Table 2.SM.2 in the electronic Supplementary Material to the IPCC Fifth Assessment report (Hartmann et al., 2013), except for South Korea (Lee et al., 2013), Mt. Cimone, Italy (Cristofanelli et al., 2014), Verkykkop, South Africa (Balashov et al., 2014) and Ushuaia, Argentina (this study, Table 1). A discussion of the uncertainties related to the calculation of long-term ozone trends can be found in the Appendix. In most regions of the world the selected monitoring sites are from remote or rural locations in an effort to characterize regional ozone trends, while urban sites were not considered due to their tendency to be strongly affected by local emissions. The exception to this rule is for East Asia where long-term ozone records are extremely limited. Therefore to learn what is possible from the region of the planet with the fastest growing ozone precursor emissions (Granier et al., 2011), East Asian long-term ozone monitoring sites were included, regardless of their urban or rural status.

Figure 2a shows all available surface and lower tropospheric ozone trends that began between 1950–1979 and ended between 2000–2010. There are thirteen records in the NH with two, Arkona-Zingst and Arosa, beginning in the 1950s. All of the NH sites indicate increasing ozone with 11 sites having statistically significant trends of 1–5 ppbv decade$^{-1}$, corresponding to >100% ozone increases since the 1950s, and 9–55% ozone increases since the 1970s. In the SH only 6 sites are available, all indicating increasing ozone with 3 having statistically significant trends of 2 ppbv decade$^{-1}$. Ozone monitoring in the free troposphere since the 1970s is even more limited. Significant positive trends since 1971 have been observed using ozonesondes (balloons) above Western Europe, Japan and coastal Antarctica (rates of increase range from 1–3 ppbv decade$^{-1}$), but not at all levels (Oltmans et al., 2013). In addition, aircraft have measured significant upper tropospheric trends in one or more seasons above the northeastern USA, the North Atlantic Ocean, Europe, the Middle East, northern India, southern China and Japan (Schnadt Poberaj et al., 2009). Insignificant free tropospheric trends were found above the Mid-Atlantic USA (1971–2010) (Oltmans et al., 2013) and in the

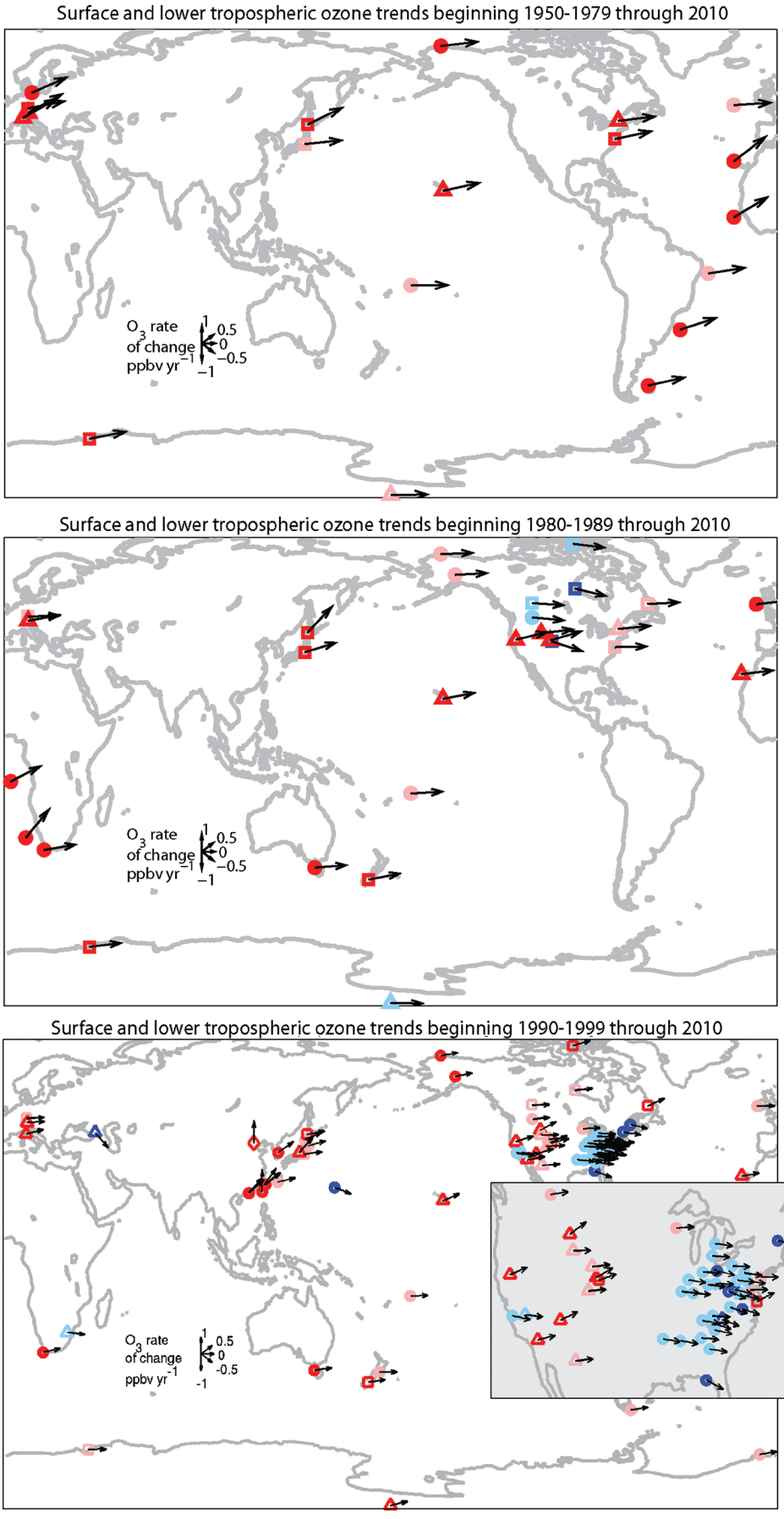


## Figure 2

**Global surface and lower tropospheric ozone trends.**

a) Ozone trends based on yearly average ozone values (using all hours of the day) at the surface or within the lower troposphere, beginning between 1950–1979 and ending between 2000–2010. b) as in a) but for trends beginning between 1980–1989 and ending between 2000–2010. c) as in a) but for trends beginning between 1990–1999 and ending between 2000–2010, with inset providing a close-up of trends in the USA. Most of the sites are in rural locations so that they are representative of regional air quality, however many of the Asian sites are urban. Measurements were made at the surface below 1 km (circles), at the surface above 1 km (triangles), in the lower troposphere by ozonesondes (squares) and in the lower troposphere by aircraft (diamonds). Vectors indicate the ozone rate of change at each site, ppbv $yr^{-1}$, as shown in the legend. Colors indicate ozone trends that are statistically significant and positive (red), statistically insignificant and positive (pink), statistically insignificant and negative (light blue) and statistically significant and negative (blue). The ozone trend values and 95% confidence limits are listed in the Electronic Supplement to the IPCC Fifth Assessment report, except for South Korea (1990–2010) (Lee et al., 2013), Mt. Cimone, Italy (1991–2011) (Cristofanelli et al., 2014) Verkykkop, South Africa (1990–2007) (Balashov et al., 2014), and Ushuaia, Argentina (this study).

Listed below are the publications that provided trend values for each panel:

a) Lelieveld et al. (2004); Parrish et al. (2012); Oltmans et al. (2013)

b) Lelieveld et al. (2004); Parrish et al. (2012); Oltmans et al. (2013)

c) Helmig et al. (2007); Ding et al. (2008); Tarasova et al. (2009); Wang et al. (2009); Li et al. (2010); Lin et al. (2010); Cooper et al. (2012); Parrish et al. (2012); Lee et al. (2013); Oltmans et al. (2013); Balashov et al. (2014); Cristofanelli et al. (2014).

doi: 10.12952/journal.elementa.000029.f002

**Table 2. Daytime (11:00 – 16:59 local time) ozone trends based on seasonal median values at 6 US and 2 European rural sites between 1990 and 2010.** Trends are reported in units of ppbv $yr^{-1}$ with the 95% confidence limit and p-value indicated. Statistically significant trends ($p < 0.05$) are in bold font.

| Site | Spring (MAM) | Summer (JJA) | Winter (DJF) |
|---|---|---|---|
| Lassen Volcanic National Park, CA | **0.39 ± 0.15, p = 0.00** | 0.22 ± 0.28, p = 0.11 | **0.21 ± 0.14, p = 0.01** |
| Joshua Tree National Park, CA | **0.31 ± 0.25, p = 0.02** | 0.23 ± 0.32, p = 0.16 | 0.14 ± 0.19, p = 0.12 |
| Gothic, Colorado | 0.01 ± 0.20, p = 0.89 | –0.01 ± 0.27, p = 0.96 | –0.02 ± 0.12, p = 0.72 |
| Whiteface Mtn. Summit, New York | –0.02 ± 0.32, p = 0.91 | **–0.48 ± 0.18, p = 0.00** | 0.09 ± 0.20, p = 0.34 |
| Big Meadows, Shenandoah NP, VA | 0.00 ± 0.20, p = 0.97 | **–0.70 ± 0.33, p = 0.00** | **0.14 ± 0.13, p = 0.03** |
| Beltsville, MD | 0.00 ± 0.21, p = 0.98 | **–0.66 ± 0.33, p = 0.00** | **0.30 ± 0.20, p = 0.01** |
| Hohenpeissenberg, Germany | 0.16 ± 0.23, p = 0.16 | –0.28 ± 0.37, p = 0.14 | **0.19 ± 0.19, p = 0.05** |
| *Ispra, Italy | **–0.40 ± 0.31, p = 0.01** | **–1.09 ± 0.43, p = 0.00** | 0.02 ± 0.29, p = 0.88 |

*Annual trend at Ispra using:
daytime values (11–16 local time) and all months of the year: –0.23 ± 0.25, p=0.07
nighttime values (00–05 local time) and all months of the year: 0.33 ± 0.24, p=0.01
all hourly values and all months of the year: 0.16 ± 0.23, p=0.17
doi:10.12952/journal.elementa.000029.t002

upper troposphere above the western USA (1975–2001) (Schnadt Poberaj et al., 2009). While the available data in the free troposphere are limited, a notable finding from the existing literature is that no site or region has shown a significant negative ozone trend since the 1970s.

Surface and boundary layer ozone trends beginning between 1980–1989 and ending between 2000–2010 are shown in Figure 2b. More sites are available for this time period compared to the trend analysis in Figure 2a. The NH sites increased to twenty but not all show increasing ozone. For this period 15 sites have increasing ozone (9 statistically significant) while 5 sites have decreasing ozone (2 statistically significant). Interestingly all of the decreasing ozone trends are in central North America, perhaps indicating a regional shift in transport pathway that temporarily affected ozone (Tarasick et al., 2005). Eight sites are available in the SH with 6 having statistically significant positive trends.

Reported ozone trends that began in the 1990s are much more numerous than previous decades, especially in the USA due to the many rural monitoring sites established by the US National Park Service and The Clean Air Status and Trends Network (CASTNET) (Cooper et al., 2012). Figure 2c shows that surface ozone trends vary regionally for the period 1990–2010. In Europe ozone generally increased through much of the 1990s but has leveled off or decreased since 2000 at rural and mountaintop sites and at Mace Head on the west coast of Ireland (Tarasova et al. 2009; Gilge et al., 2010; Logan et al. 2012; Parrish et al. 2012; Derwent et al., 2013; Oltmans et al. 2013). In North America surface ozone has increased in eastern and Arctic Canada, but is unchanged in central and western Canada (Oltmans et al. 2013). Surface ozone has increased in baseline air masses coming ashore in the marine boundary layer along the US west coast (Parrish et al. 2012). Further inland ozone increased at half of the rural sites in the western United States during spring (Cooper et al., 2012). Across the United States the yearly average ozone trends shown in Figure 2c using measurements from all hours of the day mask differing seasonal trends based on daytime measurements when the boundary layer is well mixed (Cooper et al., 2012). In the eastern US surface ozone has decreased strongly in summer especially for extreme events (Lefohn et al. 2010), is largely unchanged in spring, and has increased in winter, while ozone increases in the western US are strongest in spring (Cooper et al. 2012). East Asian surface ozone is generally increasing (Ding et al. 2008; Wang et al., 2009; Li et al., 2010; Lin et al., 2010; Parrish et al., 2012; Oltmans et al., 2013). Downwind from Asia, ozone is increasing in the lower free troposphere at Mauna Loa, Hawaii (Lin et al., 2014), but decreasing at the remote marine boundary layer site of Minamitorishima, Japan (Oltmans et al., 2013). In the SH ozone has increased at eight of the nine available sites, although trends are significant at only four sites (Helmig et al., 2007; Oltmans et al., 2013). One final conclusion regarding surface ozone trends is that positive trends at northern mid-latitudes, where anthropogenic emissions are highest, are greater than those in other latitude bands, as previously noted by Zellner and Gesellschaft Deutscher Chemiker (2011) (see their Figure 14, page 94). Accordingly, present-day yearly average ozone mixing ratios in the northern mid-latitudes are notably greater than at southern mid-latitudes (Figure 1), a clear difference that did not exist in the early 1970s (Fabian and Pruchniewicz, 1977.

Focusing on the free troposphere during 1990–2010, ozonesonde observations are most reliable since the mid-1990s due to methodological changes in measurement techniques (Logan et al., 2012). Ozone has decreased above Europe since 1998 (Logan et al. 2012) and is largely unchanged above Japan (Oltmans et al. 2013). Otherwise, the rest of the regions with measurements (North America, North Pacific Ocean, SH) show a mix of positive trends (both significant and insignificant) depending on altitude, with no site having a negative trend at any altitude. Although not shown in Figure 2, a springtime analysis of mid-tropospheric ozone above western North America reveals a significant increase from 1995 to 2011 (Cooper et al., 2012).

While Figure 2 indicates that surface and boundary layer ozone has generally increased around the globe since the 1950s and 1970s, with recent decreases in parts of the eastern USA and a leveling off of ozone mixing ratios in western Europe, broad regions of the globe are not represented due to the relatively sparse monitoring network. Some additional insight into ozone trends above the remote regions of the North and South Pacific Oceans and the entire tropical band can be gained from analysis of satellite-detected tropospheric column ozone measurements. Tropospheric column ozone measured by the Total Ozone Mapping Spectrometer (TOMS) and analyzed using the cloud-slicing technique found no trend over the tropical Pacific Ocean but significant positive trends (5–9% decade$^{-1}$) in the mid-latitude Pacific of both hemispheres during 1979–2003 (Ziemke et al., 2005). Beig and Singh (2007) using a different method to determine TOMS tropospheric column ozone (1979–2005) found significant positive trends (2–9% decade$^{-1}$) across broad regions of the tropical South Atlantic, India, southern China, southeast Asia, Indonesia and the tropical/subtropical regions downwind of China.

## 4. Present day ozone distribution based on OMI/MLS retrievals

Today, surface ozone is monitored routinely at thousands of sites around the world. In contrast, routine vertical profiling is limited to a few dozen ozonesonde and lidar sites and a few airports that are frequented by commercial aircraft equipped with air pollution monitoring equipment (Europe's IAGOS program: www.iagos.org) (see Figure 2.27 in Dentener et al., 2011). While present day ozone monitoring is more extensive than at any time in the past, broad regions of the globe such as the oceans, polar regions, and sparsely populated areas have few or no in situ ozone measurements. The scarcity of surface and vertical ozone measurements across much of the Earth, and ozone's high spatial and temporal variability, prevents the construction of a comprehensive global survey of boundary layer and free tropospheric ozone from in situ observations. Fortunately, recent advances in satellite detection methods allow for satellite-based quantifications of the tropospheric ozone burden across much of the Earth.

An assessment of the near-global (70°S–70°N) tropospheric ozone burden has been derived from instruments onboard NASA's polar orbiting Aura satellite that has monitored stratospheric ozone and tropospheric trace gases since 2004. The Ozone Monitoring Instrument (OMI) Science Team combines OMI total ozone measurements (troposphere and stratosphere) with Microwave Limb Sounder (MLS) stratospheric column ozone measurements to produce global maps of tropospheric column ozone (TCO) (Ziemke et al. 2006). TCO is expressed in Dobson Units (DU), where 1 DU is the number of molecules of ozone per square centimeter required to create a layer of pure ozone 0.01 millimeters thick at standard temperature and pressure (or $2.69\times10^{16}$ ozone molecules cm$^{-2}$). Comparison of OMI/MLS TCO to tropospheric ozonesonde observations shows that the satellite product captures the seasonal cycle and spatial distribution of the observations (Ziemke et al., 2011). Between 25°S and 50°N annual mean tropospheric ozone mixing ratios are very similar: 48.8 ppbv from the ozonesondes, 47.0 ppbv from OMI/MLS, and a correlation coefficient of 0.94. However, at high latitudes OMI/MLS is biased high by as much as 25% for some ozonesonde stations.

As illustrated by the OMI/MLS TCO climatology (Ziemke et al., 2011) in Figure 3, the NH experiences its peak ozone values during boreal summer at mid-latitudes. The SH peak occurs in austral spring in the tropics and subtropics between South America and Africa and in a band centered at 25°S–30°S stretching from southern Africa eastward to Australia. On an annual basis NH average TCO exceeds the SH average by 4%, 12%, and 18% at low (0°–25°), mid- (25°–50°), and high (50°–60°) latitudes, respectively (based on Table 3 from Ziemke et al. [2011]). Comparing the two hemispheres with a slightly different quantification, 52% of the annual average near-global (70° S – 70° N) tropospheric ozone burden (314 Tg) resides in the NH while 48% resides in the SH, which equates to an 8% enhancement in the NH relative to the mean SH burden (Figure 4). In general both hemispheres have a spring maximum and autumn minimum in tropospheric ozone burden.

A complication of the OMI/MLS TCO quantity is that it is sensitive to the depth of the troposphere. A region with a relatively high tropopause will show greater TCO values than an adjacent region with a lower tropopause assuming the ozone concentrations throughout the troposphere are similar. Additionally TCO values above regions of high terrain such as the western USA, the Tibetan Plateau and the Andes are lower than adjacent regions due to the limited depth of the troposphere. A method for removing these biases is to convert the TCO values to units of ppbv. The resulting ozone mixing ratios do not apply to any particular altitude but should be thought of as the ozone mixing ratio in a vertically well-mixed column of air. Comparison of the TCO mixing ratios in Figure 5 to the standard TCO values in Figure 3 shows that the very low TCO values above the western USA, the Tibetan Plateau and the Andes are no longer present in Figure 5, albeit the TCO mixing ratios above these regions are now enhanced because the columns are biased towards higher altitudes. Converting TCO from DU to ppbv increases the ozone enhancement of the NH relative to the SH from 8% (based on the hemispheric mass burdens, as discussed above) to 13%, due to the higher elevation of the NH land surfaces.

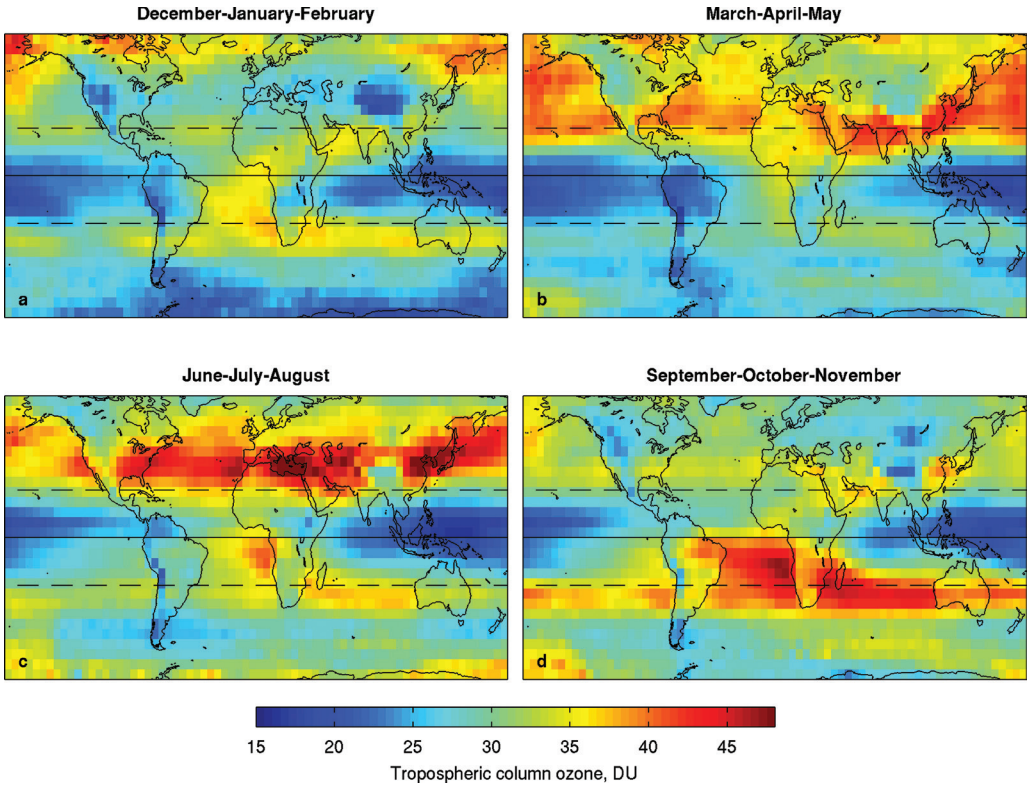


## Figure 3

**OMI/MLS tropospheric column ozone by season.**

The data are averaged over the period October 2004 – December 2010 and reported at 5° × 5° horizontal resolution. Locations of the equator (solid horizontal line) and tropics (dashed horizontal lines) are indicated.

doi: 10.12952/journal.elementa.000029.f003

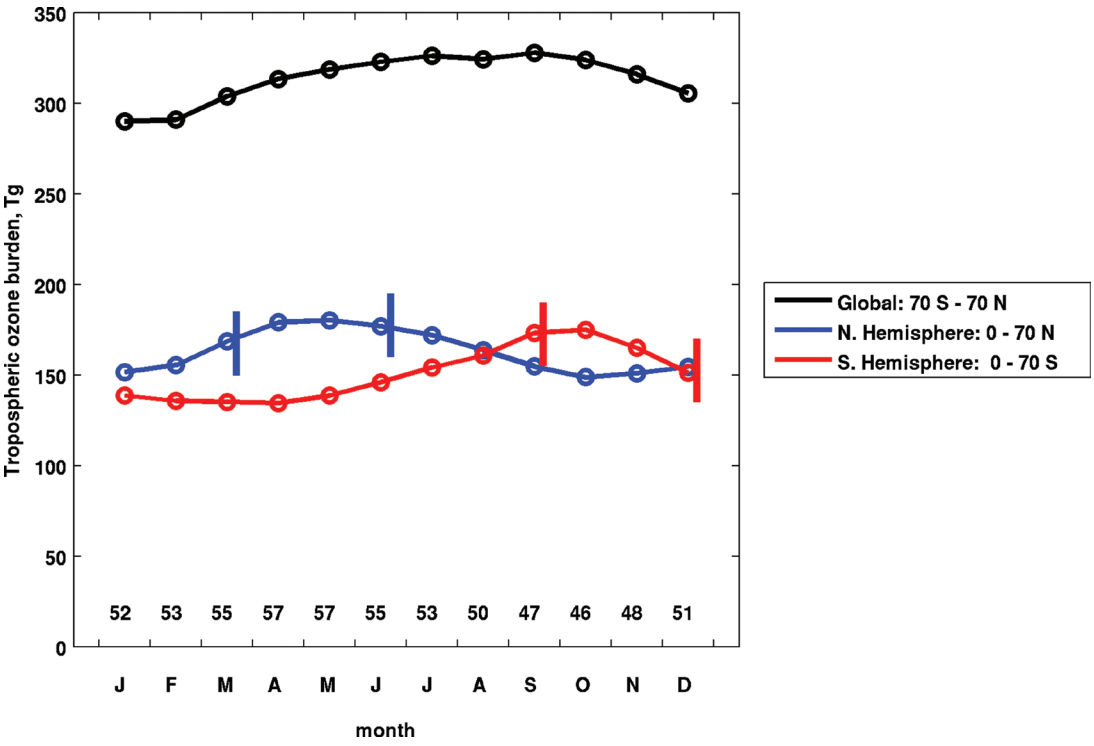


## Figure 4

**OMI/MLS detected tropospheric ozone burden for the globe and each hemisphere.**

The mass of tropospheric ozone (Tg) is shown by month for the globe (70° S – 70° N) and the Northern and Southern Hemispheres. Springtime in each hemisphere is indicated by the 3-month period between the vertical bars, beginning with the spring equinox and ending with the summer solstice. Numbers above the x-axis indicate the monthly percentage of the global tropospheric ozone burden that resides in the Northern Hemisphere.

doi: 10.12952/journal.elementa.000029.f004

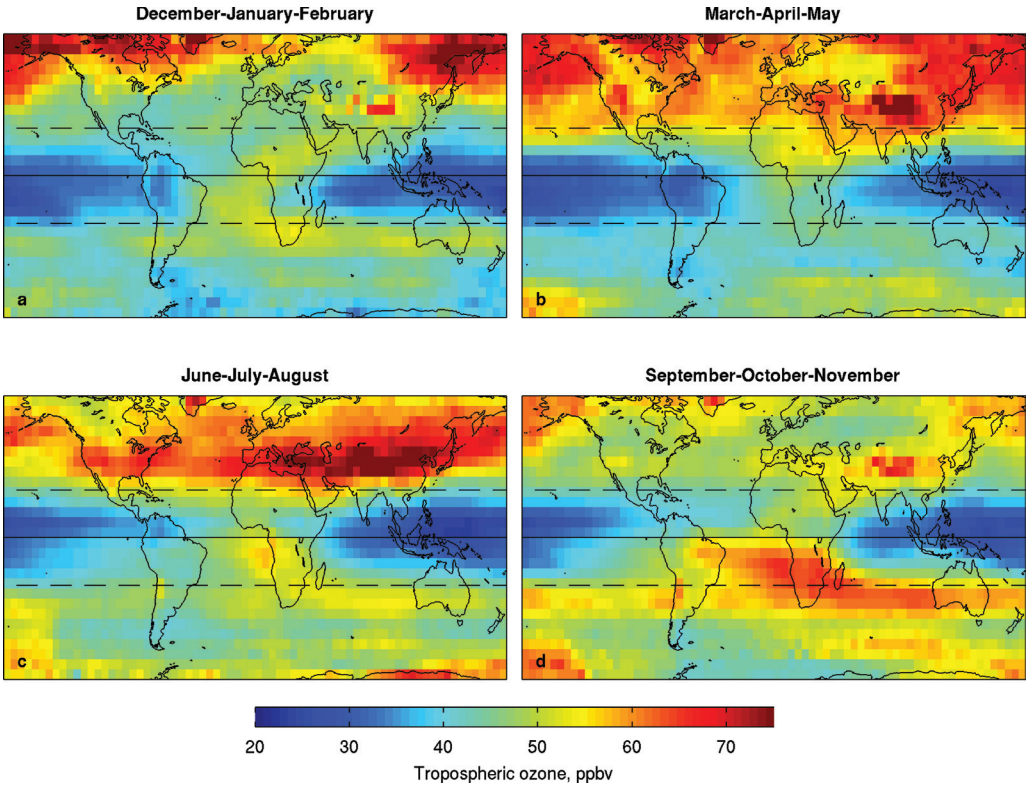


**Figure 5**

**OMI/MLS detected tropospheric ozone burden for the globe and each hemisphere, converted to ppbv.**

As in Figure 3 but the tropospheric column ozone values have been converted to units of ppbv. Locations of the equator (solid horizontal line) and tropics (dashed horizontal lines) are indicated.

doi: 10.12952/journal.elementa.000029.f005

Examination of TCO mixing ratios by latitude shows that northern extra-tropical values exceed those in the SH by 19% on an annual basis, while tropical values are similar in both hemispheres (Figure 6a, b). Many physical processes, photochemical and dynamical, determine the tropospheric ozone distribution shown in Figure 6a, b. The purpose of this paper is primarily to describe the distribution and trends of tropospheric ozone without attributing causes, but it is worthwhile to note that chemistry-climate models attribute the greater ozone burden at northern mid-latitudes to ozone production from enhanced anthropogenic emissions in the NH (Horowitz, 2003; Young et al., 2013), which contains approximately 90% of the global population and 90% of anthropogenic $NO_x$ emissions (Dentener et al., 2011). However, the hemispheric ozone burden is not proportional to $NO_x$ emissions as shown by comparing Figure 6a, b to Figure 6c. Monthly total (anthropogenic, biomass burning and lightning) $NO_x$ emissions in the NH range from 9.1 to 10.8 Tg, while SH emissions range from 1.5 to 3.4 Tg with a prominent late winter/early spring peak driven by biomass burning.

Seasonally, the NH mid-latitude TCO mixing ratios increase throughout the spring and peak in late spring and early summer (Figure 6a). In contrast the mid-latitude peak in the SH occurs in early spring with decreasing ozone values throughout the remainder of the season. The seasonal contrast between the two hemispheres is explored further in Figures 7 and 8. Maximum monthly TCO mixing ratios are generally greater at mid-latitudes in the NH than the SH, but in the tropics the greatest values are found across the South Atlantic Ocean and southern Africa. Almost all grid cells across the SH mid-latitudes have maxima that occur in early spring, but in the NH the maximum values mainly occur in late spring and early summer (Figure 8). According to chemical transport model simulations, hemispheric differences in anthropogenic emissions and photochemical ozone production lead to the NH mid-latitudes having a much higher frequency of maximum monthly surface ozone mixing ratios during summer (e.g. Box 5.2 in, The Royal Society [2008]).

## 5. Present day surface ozone distribution based on in situ observations

While the OMI/MLS TCO retrievals effectively indicate the tropospheric ozone burden, they are not sensitive to surface ozone mixing ratios (Ziemke et al., 2011). Even though many regions of the globe have no surface ozone monitoring, a rough representation of present-day (2005–2010) surface ozone variability by latitude, longitude and elevation is provided by the 20 rural or remote baseline ozone data sets shown in Figure 1. These data are yearly averages using measurements from all hours of the day, with baseline ozone defined as the observed ozone at a site when it is not influenced by recent, locally emitted or produced anthropogenic pollution, following the definition by the Task Force on Hemispheric Transport of Air Pollution (Dentener et al., 2011).

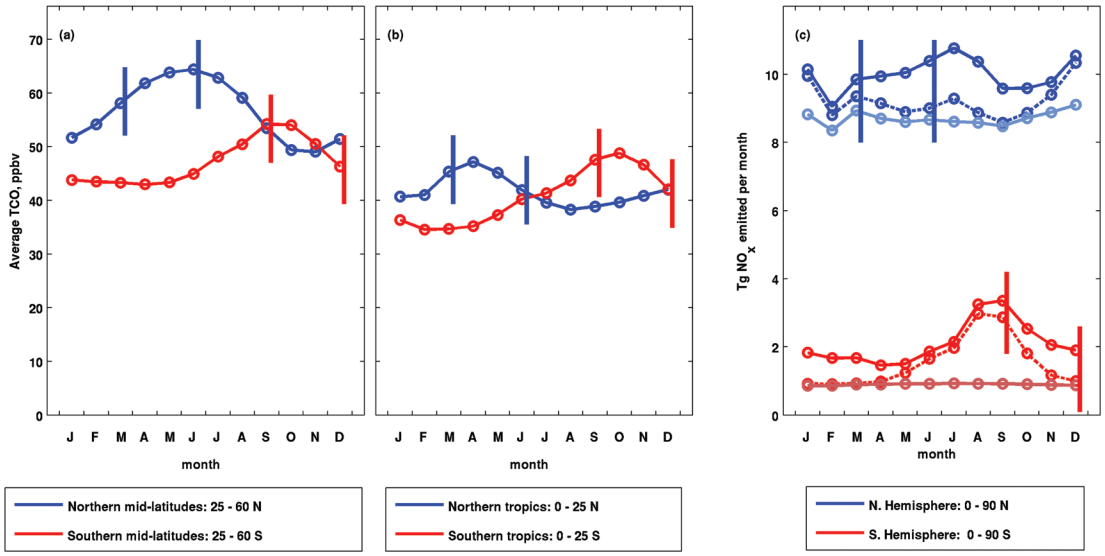


## Figure 6

**A hemispheric comparison of tropospheric ozone burden and $NO_x$ emissions.**

Monthly tropospheric column ozone (ppbv) is shown for (a) mid-latitudes and (b) the tropics. Springtime in each hemisphere is indicated by the 3-month period between the vertical bars, beginning with the spring equinox and ending with the summer solstice. c) Monthly $NO_x$ emissions (expressed as $NO_2$) shown from just anthropogenic sources in the Northern Hemisphere (light blue) and Southern Hemisphere (light red), the sum of anthropogenic and biomass burning sources in the Northern (blue dashed) and Southern Hemisphere (red dashed), and the sum of anthropogenic, biomass burning and lightning sources in the Northern (blue solid) and Southern Hemisphere (red solid). Global monthly anthopogenic emissions are for the year 2010 and include emissions from aircraft and international shipping (EDGAR HTAP_V2), while global monthly biomass burning emissions are averaged over 2005–2009 and include agricultural burning (GFED v3, (van der Werf et al., 2010)). Global lightning $NO_2$ emissions are fixed at 5 Tg N (based on the best estimate of Schumann and Huntrieser (2007)) and distributed globally according to the LIS/OTD v2.2 gridded satellite lightning data produced by the NASA LIS/OTD Science Team (Christian et al., 2003).

doi: 10.12952/journal.elementa.000029.f006

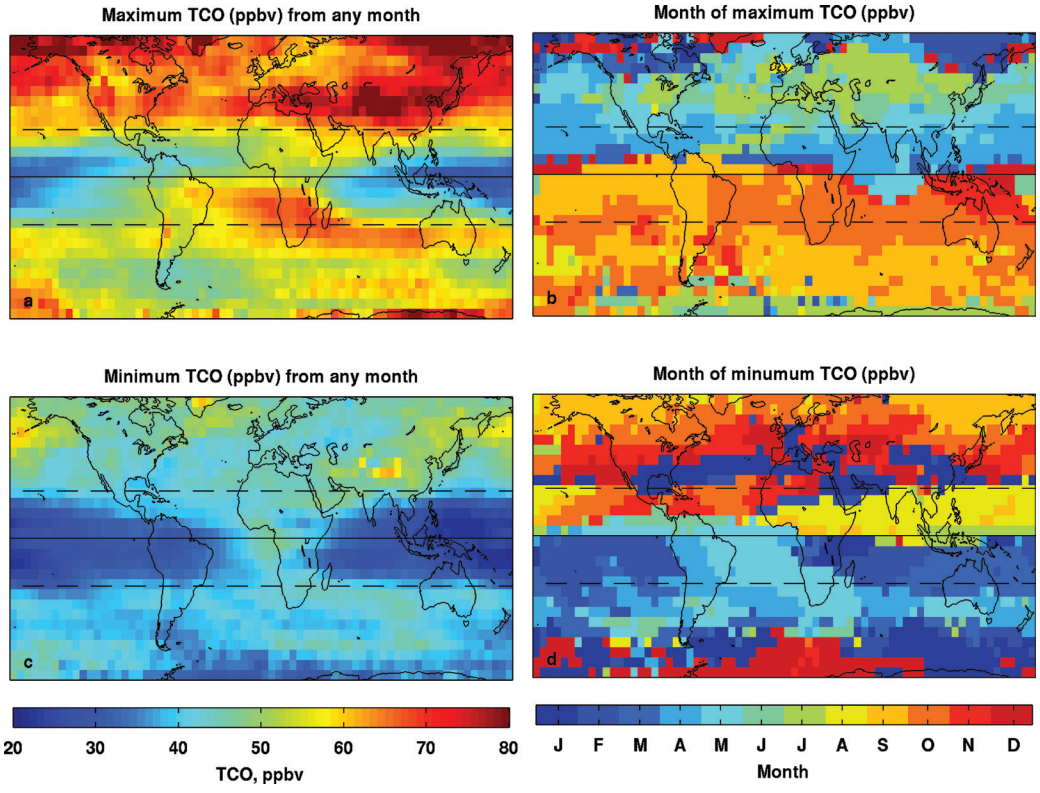


## Figure 7

**Extreme monthly TCO values around the globe and their month of occurrence.**

The maximum TCO value (ppbv) from any month is plotted for each 5°×5° grid cell (a) and the month in which the maximum value occurs is plotted in (b). Similarly, the minimum TCO value (ppbv) from any month is plotted for each 5°×5° grid cell (c) and the month in which the minimum value occurs is plotted in (d).

doi: 10.12952/journal.elementa.000029.f007

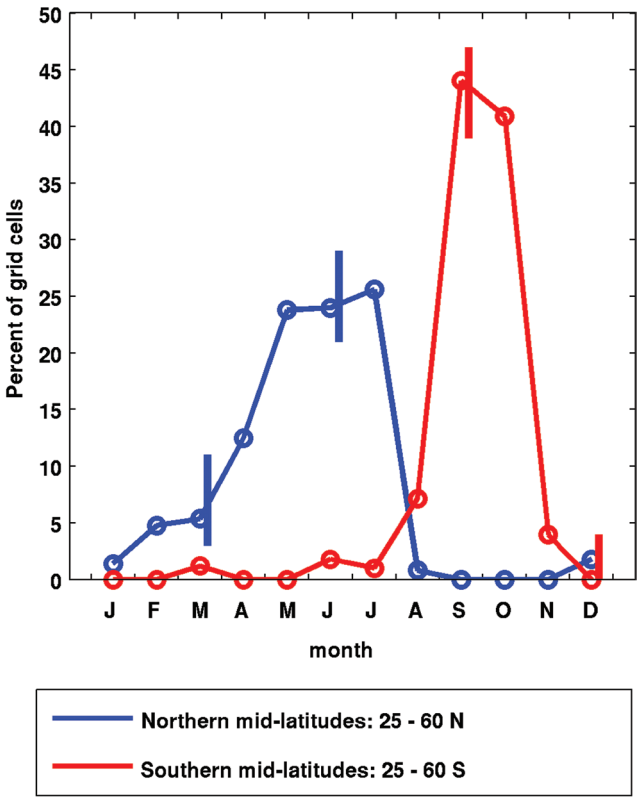


**Figure 8**
**Month of maximum TCO.**

This histogram pertains to the "Month of maximum TCO (ppbv)" at mid-latitudes, as shown in Figure 7b. It shows for each month the percentage of grid cells in the mid-latitude band during which a maximum TCO value occurred. Springtime in each hemisphere is indicated by the 3-month period between the vertical bars, beginning with the spring equinox and ending with the summer solstice.

doi: 10.12952/journal.elementa.000029.f008

The lowest surface ozone values are found in the marine boundary layer (MBL) of the tropical SH (Samoa, 13–14 ppbv), followed by the MBL of the SH mid-latitudes (Ushuaia, Argentina, 24–25 ppbv; Cape Point, South Africa, 24–26 ppbv; Cape Grim, Tasmania, 24–26 ppbv) and high latitudes (Arrival Heights, Antarctica, 26–27 ppbv). The only extratropical site in the NH with such low ozone values is the coastal site of Barrow, Alaska (27–28 ppbv), where bromine released from the Arctic Ocean severely depletes springtime ozone (Oltmans et al., 2012); the only high elevation site in either hemisphere with ozone as low as these MBL sites is the South Pole (29–31 ppbv at 2.8 km a.s.l.). Proceeding to the MBL of northern mid-latitudes, ozone ranges from 28–31 ppbv at Arkona-Zingst on the northern German coast, 33–37 ppbv on the US west coast, 38–40 at Storhofdi, Iceland, 40–41 ppbv at Mace Head, Ireland, and 43–49 ppbv along the Japanese west coast. At high elevations in the NH ozone ranges from 38–46 ppbv in the tropics (Mauna Loa at 3.4 km a.s.l.), 37–43 ppbv in southern Germany (Hohenpeissenberg at 1 km a.s.l.) and the Swiss valley-bottom site of Arosa (1.8 km a.s.l.), 40–44 ppbv at Lassen Volcanic National Park in northern California (1.8 km a.s.l.), 45–48 ppbv at Summit, Greenland (3.2 km a.s.l.) 49–52 ppbv at Zugspitze, southern Germany (3.0 km a.s.l.), 52–54 ppbv at Jungfraujoch, Switzerland (3.6 km a.s.l.), and 50–59 ppbv at Mt. Happo, western Japan (1.9 km a.s.l). In both the MBL and at high elevations in the NH, the greatest ozone mixing ratios are found in western Japan, immediately downwind of continental East Asia where ozone precursor emissions have increased rapidly since 1980 (Granier et al., 2011; Lee et al., 2013).

The sites shown in Figure 1 are continental or marine baseline monitoring sites representative of rural or remote regions, far from fresh anthropogenic ozone precursor emissions. The only exception is Hohenpeissenberg located in the atmospheric boundary layer of heavily populated southern Germany, however its location on top of an isolated hill does make the site representative of central western Europe rather than any particular urban region (Gilge et al., 2010). To contrast ozone at these continental and marine baseline sites with ozone in polluted regions of the NH mid-latitudes, five rural sites in East Asia, the western USA, the eastern USA and western Europe were selected (Figure 9):

1) Western Europe: The JRC Ispra EMEP station is located on the campus of the Joint Research Center-Ispra (45.8°N, 8.6°E, 209 m a.s.l.). The site is in a semi-rural area of the Po Valley in northern Italy, situated approximately 60 km northwest of Milan on the southern edge of the Alps. The Po Valley typically experiences the most extreme ozone concentrations in Europe (European Environment Agency, 2013) although peak ozone values have decreased strongly at Ispra since 1990 in response to emissions controls (Derwent and Hjellbrekke, 2013).
2) Western Europe: The Hohenpeissenberg Meteorological Observatory (47.8°N, 11.2°E, 985 m a.s.l.), operated by Deutsche Wetterdienst, is a WMO Global Atmosphere Watch station, located approximately

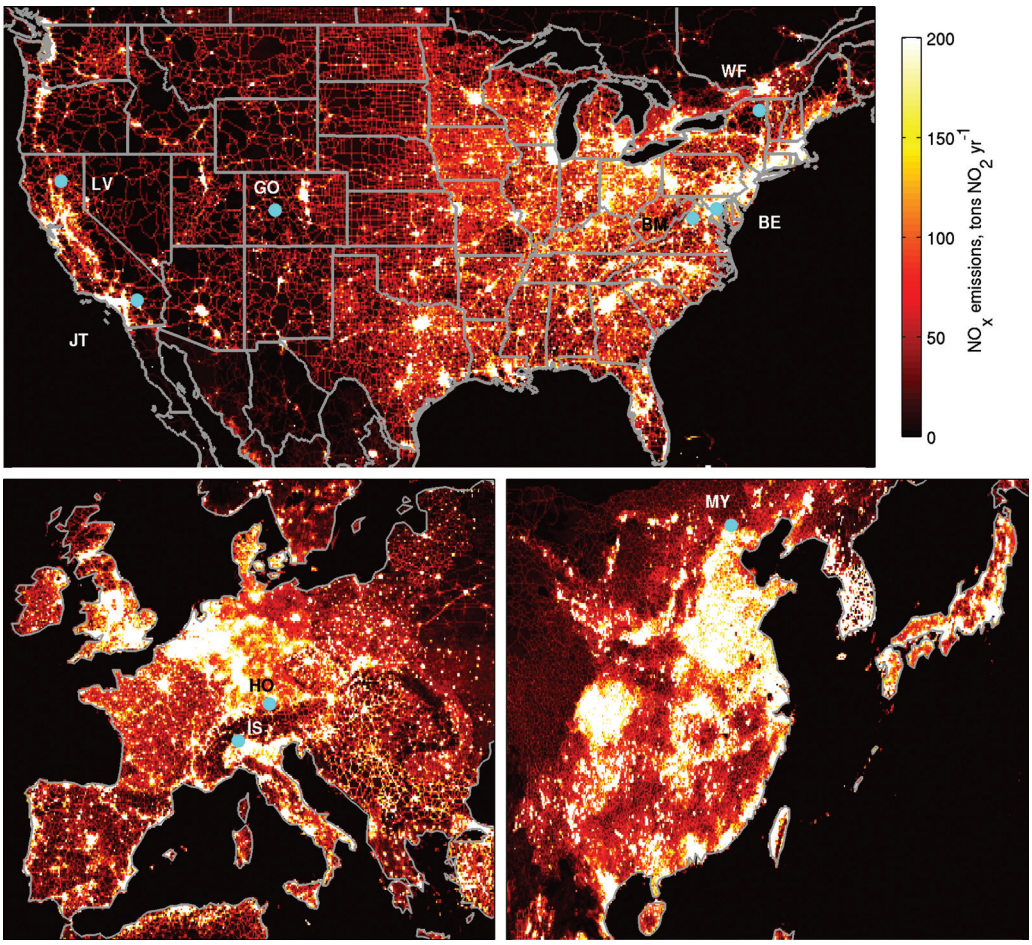


## Figure 9

**Annual anthropogenic $NO_x$ emissions for selected regions.**

$NO_x$ emissions (tons $NO_2$ $yr^{-1}$ per $0.1^\circ \times 0.1^\circ$ grid cell) across the USA (top), Europe (bottom left) and East Asia (bottom right) for the year 2005 (EDGARv4.1). Locations of several rural surface ozone monitoring sites are also indicated (blue dots): Lassen Volcanic National Park, California (LV), Joshua Tree National Park, California (JT), Gothic, Colorado (GO), Whiteface Mountain summit, New York (WF), Big Meadows, Shenandoah National Park, Virginia (BM), Beltsville, Maryland (BE), Hohenpeissenberg, Germany (HO), Ispra, Italy (IS), and Miyun, China (MY).

doi: 10.12952/journal.elementa.000029.f009

40 km north of the Alps at the summit of a solitary hill which rises 300–400 m above the surrounding rural countryside (Gilge et al., 2010).

3) China: The Miyun site (40.5°N, 116.8°E, 152 m a.s.l.) is located on the northern edge of the North China Plain about 100 km northeast of central Beijing, on the southern edge of the steep Yanshan Mountain Range. The region surrounding the site is characterized by a mix of agriculture and small villages (Wang et al., 2010).
4) Western USA: Joshua Tree National Park is located in the desert region of southern California, east and downwind of the Los Angeles Basin. Ozone measurements were made at the Lost Horse Ranger Station site from 1990 until September 1993, when the monitor was moved to the Black Rock site, 20 km to the northwest (34.1° N, 116.4° W, 1244 m a.s.l.). The terrain is similar for the two sites but the new location is closer to urban areas. While these sites are rural, air quality in the park is strongly affected by air pollution transport from the Los Angeles Basin which regularly places the rural park in exceedance of the U.S. National Ambient Air Quality Standard for ozone (Sullivan et al., 2001; Rosenthal et al., 2003; Langford et al., 2010).
5) Eastern USA: The Beltsville, Maryland ozone monitor, maintained by The US EPA's Clean Air Status and Trends Network (CASTNET), is located in a forested, rural area between Washington, DC and Baltimore, Maryland (39.0° N, 76.8° W, 46 m a.s.l.). This region of the U.S. Mid-Atlantic has experienced strong decreases in ozone and ozone precursors since the 1990s (He et al., 2013).

Figure 10 compares monthly 5$^{th}$, 50$^{th}$ and 95$^{th}$ midday ozone percentiles at these five sites during 2005–2010. At the 5$^{th}$ percentile four of the sites have ozone values less than 20 ppbv in winter and less than 40 ppbv in summer. By far the greatest 5$^{th}$ percentile values occur at Joshua Tree (35–55 ppbv), most likely due to its high elevation and deep daytime boundary layer, which can reach 4 km a.s.l. during spring and summer allowing lower free tropospheric ozone to be mixed down to the surface (Cooper et al., 2011). At the 50$^{th}$ percentile the two European sites have the lowest summer ozone values, with greater values at Beltsville, Maryland, and Joshua Tree (peaking at 73 ppbv in June) and the highest values at Miyun, China (peaking at 93 ppbv in June). A similar ranking of the sites applies to the 95$^{th}$ percentile, but at these extreme values Miyun has exceptionally high ozone, ranging from 100 ppbv to 162 ppbv during April-September.

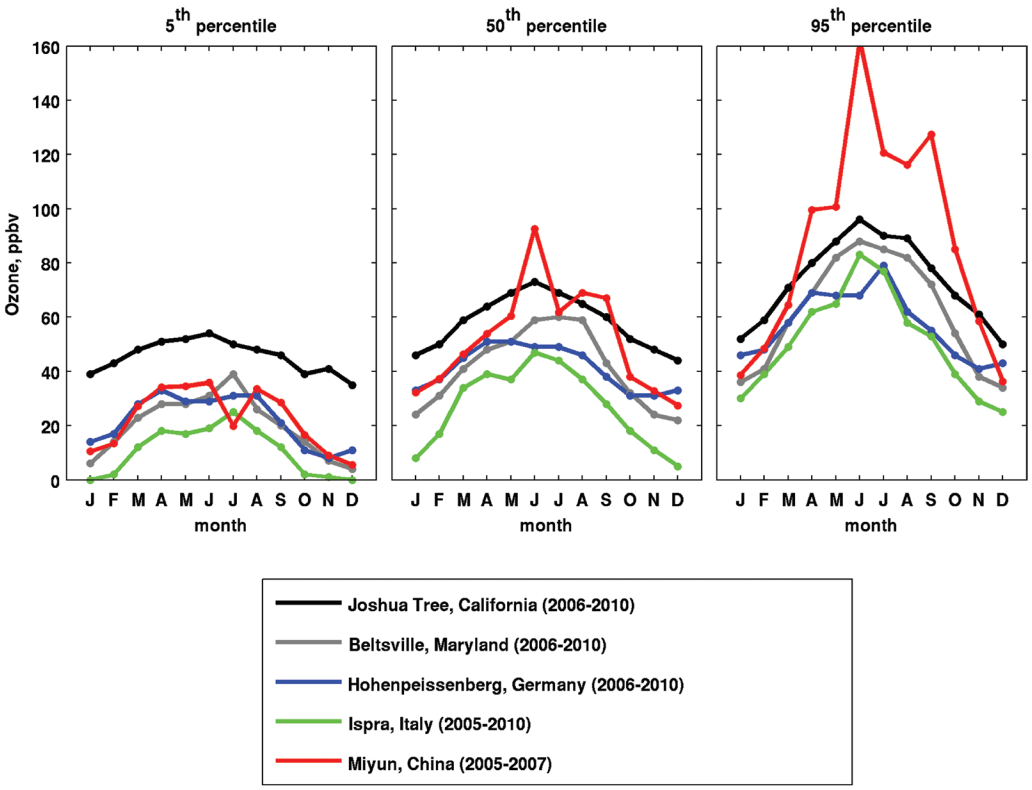


**Figure 10**

**Monthly ozone values at rural sites in the USA, Europe and China.**

Comparison of monthly 5th (left), 50th (center) and 95th (right) midday ozone percentiles at five rural sites in regions with strong emissions of ozone precursors.

doi: 10.12952/journal.elementa.000029.f010

The above comparison shows that the Miyun site in China has, by far, the greatest summertime ozone mixing ratios. We know of no rural site in the USA or Europe with such high summertime ozone mixing ratios (Cooper et al., 2012; Derwent and Hjellbreke, 2013). Comparison of the 2005–2007 midday, summertime (June, July, August) median ozone mixing ratio at Miyun (75 ppbv) to midday summertime ozone measured at multiple urban sites across northern and eastern China during 2010 (as reported by Tang et al. [2012]) indicates that the relatively high ozone values at Miyun are typical of this region. Another example of the exceptionally high ozone in northern China during June is illustrated in Figure 11 which compares partial columns of ozone and carbon monoxide (CO) in the lower troposphere (0–2 km above the surface) for 10 cities or regions in North America, Europe, the Middle East and East Asia. These measurements were made by MOZAIC commercial aircraft during June 2001–2008, and the data were processed following the procedures of Zbinden et al. (2013). Beijing stands out as having both the greatest CO and ozone values in the lower troposphere with 3–4 times greater CO, and 30–60% greater ozone compared to the other nine sites. Like China, India has a very large population and a growing economy. Ozone monitoring in India is relatively limited, however measurements are becoming more common. The highest ozone observations are typically found in the densely populated Indo-Gangetic Plain of northern India, but even here ozone is much lower than at Miyun (Ojha et al., 2012).

## 6. Seasonal shift in peak ozone

One final aspect of surface ozone that deserves discussion is the shift in the seasonal ozone cycle observed at many, but not all, rural mid-latitude monitoring sites. As discussed above, the 19th century stations that measured ozone with the Schönbein method showed that ozone most often peaked in spring, followed by winter, with some spring peaks continuing into early summer. This pattern was observed at rural and urban sites, but did not persist into the late 20th century in those regions with strong ozone precursor emissions. Marenco et al. (1994) noted that Pic du Midi had a strong springtime peak in the late 1800s that shifted to a broad spring/summer peak by the 1980s–1990s. Ozone in the center of the European continent typically experiences a summertime or broad spring/summer ozone peak, whereas sites located in less polluted regions of northern or westernmost Europe experience a springtime peak (Scheel et al., 1997; Monks et al., 2000; Wilson et al., 2012). Ozone at rural sites across the eastern United States typically peaked in summer during the 1990s (Cooper et al., 2012), while western US sites had a broader spring/summer peak. In contrast the 2006–2010 time period shows that ozone in the eastern US has strongly decreased in summer while remaining constant in spring so that the summer maximum has been replaced by a broad spring/summer peak. This shift

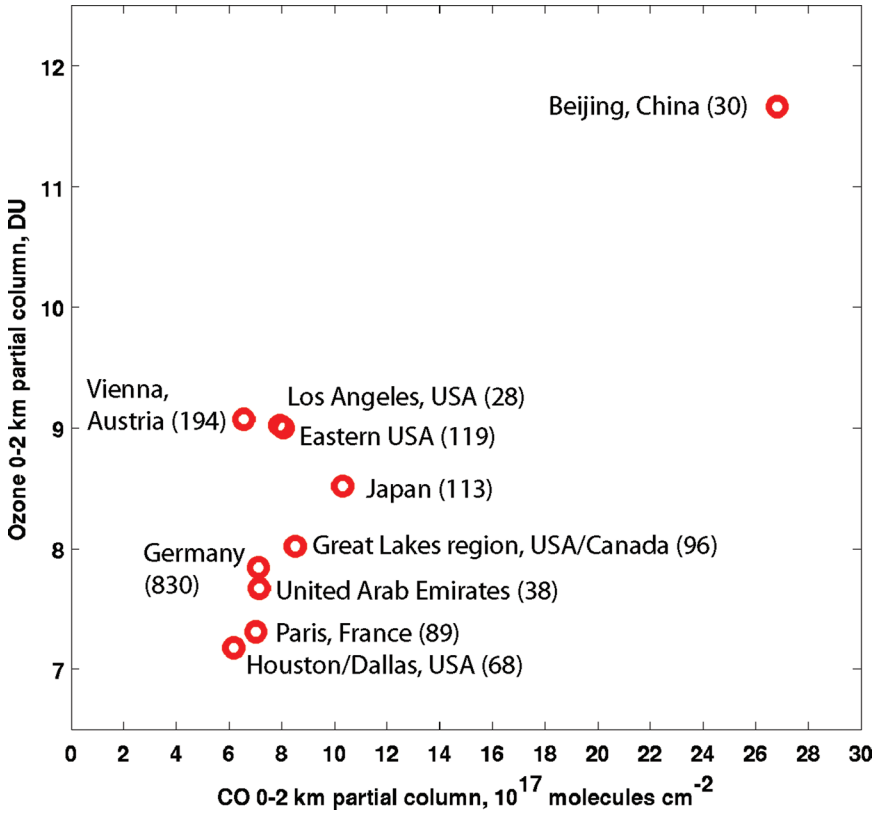


**Figure 11**

**Comparison of ozone and CO above several cities in the northern mid-latitudes.**

Partial column values of ozone (Dobson units) and CO ($10^{17}$ molecules $cm^{-2}$) during June (2001–2008) 0–2 km above the surface of 10 cities or regions in North America, Europe, the Middle East and East Asia. Numbers in parentheses indicate the number of profiles above each city or region, as measured by MOZAIC commercial aircraft.

doi: 10.12952/journal.elementa.000029.f011

in the seasonal ozone cycle appears to be a response to emissions reductions in the USA. A recent analysis by Parrish et al. (2013) examined the seasonal ozone cycle at four rural sites in Europe and one rural site in the western United States. They discovered that not only is springtime ozone greater in recent years (2005–2010) than in earlier decades (1970s through the early 1990s), but the seasonal maximum now occurs earlier in the year with 4 of the 5 sites showing a late springtime peak and Mace Head, Ireland showing a late winter peak.

To further explore the shifting seasonal ozone cycle we examine several rural sites that experience greater exposure to regional pollution than those selected by Parrish et al. (2013). Figure 12 compares the seasonal ozone cycle from 1990–1994 and 2006–2010 at the same four European and US sites shown in Figure 10. Figure 13 provides similar ozone summaries for four high elevation sites across the United States using the same data set described by Cooper et al. (2012). Beginning with Lassen Volcanic National Park in the mountains of northern California, the shift in seasonal ozone from 1990–1994 until 2006–2010 (Figure 13) is similar to Parrish et al.'s (2013) analysis of the same site (but beginning in 1988). Ozone increased significantly in winter and spring, but not in summer (Table 2), shifting ozone from a prominent peak in August to a broad spring-summer peak. At Joshua Tree springtime ozone also increased significantly while summer ozone remained far greater than in spring (Figure 12). Therefore at this site, which is strongly impacted by pollution export from the Los Angeles Basin in summer, no shift in the seasonal ozone peak was observed.

Further east, the high elevation site of Gothic in the Colorado Rocky Mountains shows no clear shift in the seasonal ozone cycle (Figure 13), retaining its late spring peak. In the eastern US the high elevation sites of Big Meadows in Shenandoah National Park, Virginia and Whiteface Mountain Summit in northern New York State experienced strong decreases in summertime ozone and no significant increase in springtime ozone (Table 2) shifting the ozone peak from summer to spring (Figure 13). The low-elevation eastern US site of Beltsville, Maryland also saw strong decreases in summertime ozone but a shift in the ozone peak only occurred at the 95$^{th}$ percentile, from July to June. We note here that summertime ozone decreases, especially during high ozone events, are a widespread phenomenon across the eastern United States at both rural and urban sites, and are a response to effective ozone precursor emission controls (Frost et al., 2006; Kim et al., 2006; Gilliland et al., 2008; U.S. Environmental Protection Agency, 2009; Lefohn et al., 2010; Butler et al., 2011; Hogrefe et al., 2011; Pozzoli et al., 2011; Cooper et al., 2012; He et al., 2013; Rieder et al., 2013).

In western Europe median ozone at Hohenpeissenberg shifted from a summer to a spring peak from 1990–2010 but not as strongly as the shift noted by Parrish et al. (2013) during 1971–2010. At Ispra, Italy (Figure 12) ozone observations at the 50$^{th}$ and 95$^{th}$ percentiles peaked in July in the early 1990s but now peak in June due to very strong ozone decreases in summer (Table 2).

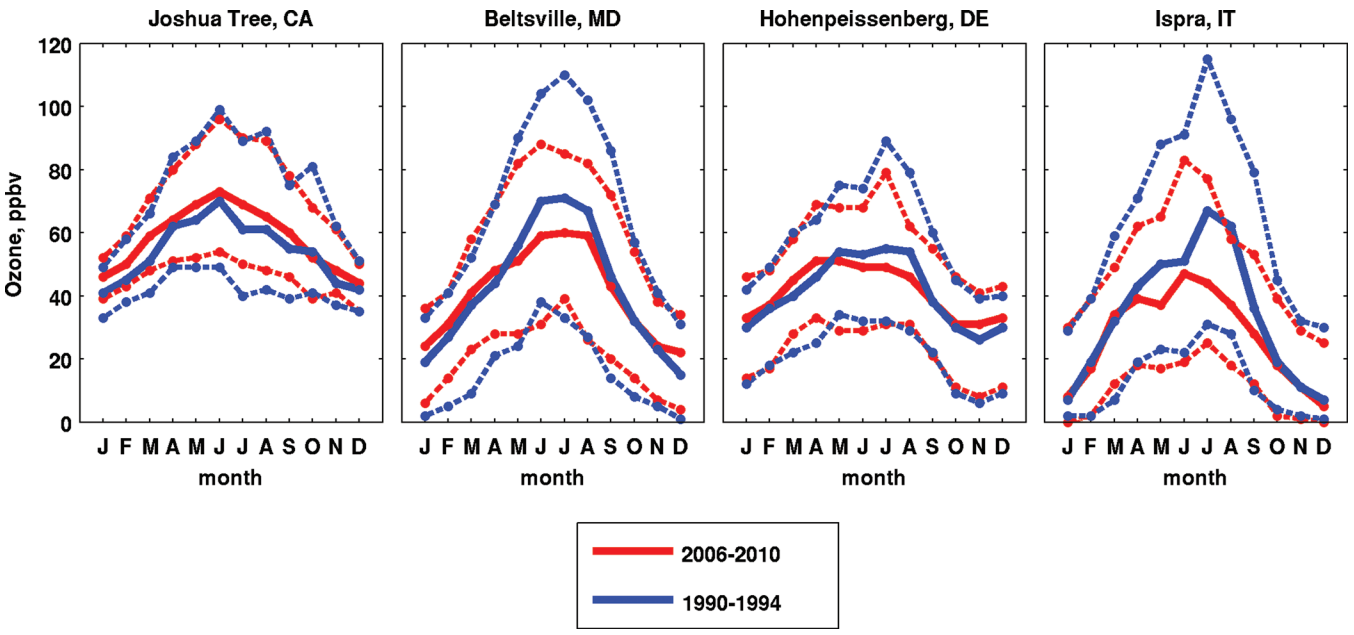


## Figure 12

**Changes in the seasonal cycle of ozone at four rural surface sites.**

Monthly daytime 50$^{th}$ (solid lines), 5$^{th}$ (lower dashed lines) and 95$^{th}$ (upper dashed lines) ozone percentiles for 1990–1994 and 2006–2010 at four rural surface sites in the USA and Europe.

doi: 10.12952/journal.elementa.000029.f012

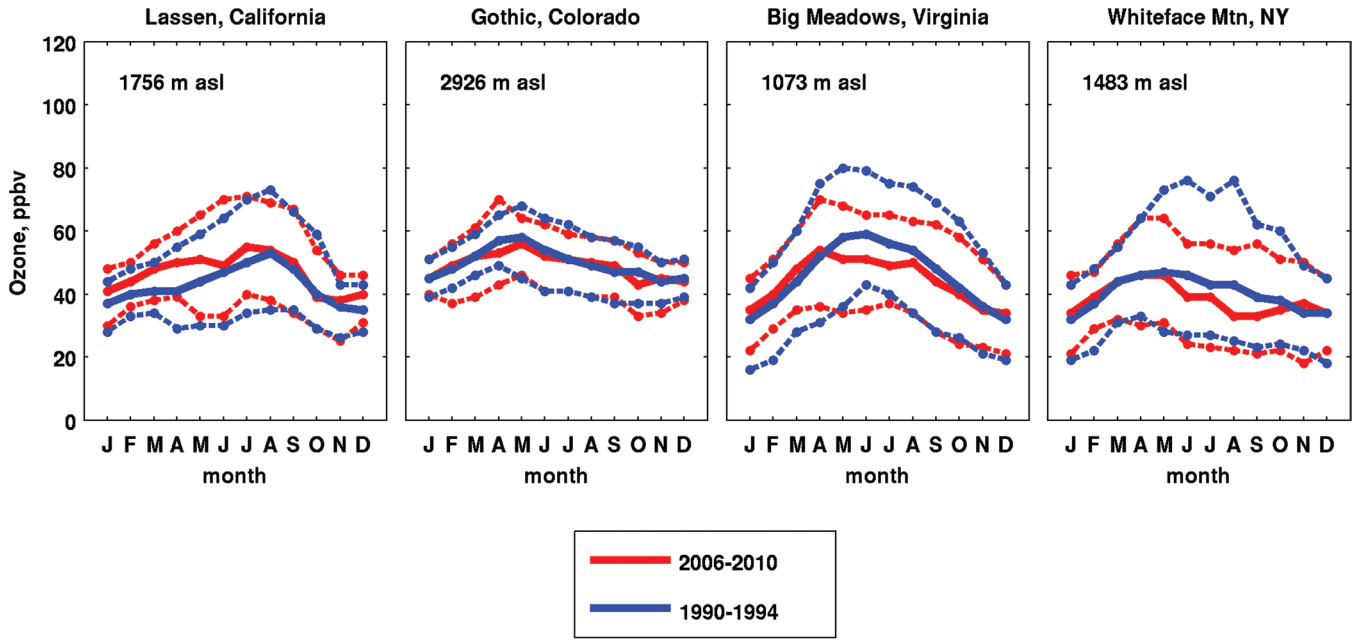


## Figure 13

**Changes in the seasonal cycle of ozone at four US mountain sites.**

Monthly daytime 50$^{th}$ (solid lines), 5$^{th}$ (lower dashed lines) and 95$^{th}$ (upper dashed lines) ozone percentiles for 1990–1994 and 2006–2010 at four rural, high elevation, surface sites across the USA.

doi: 10.12952/journal.elementa.000029.f013

This analysis shows that the seasonal ozone cycle at northern mid-latitudes has generally changed over the 1990–2010 period, but not at all sites. The three sites with no shift in the seasonal ozone cycle (based on monthly median values) were the polluted sites of Joshua Tree and Beltsville, which still experience very strong ozone pollution episodes in summer, and Gothic, which retains its springtime peak and is not impacted by strong summertime ozone events. The other 5 sites now experience peak ozone 1–3 months earlier in the year. The reason for the shift is due to either a decrease in summertime ozone, an increase in springtime ozone or a combination of the two. Additional studies are required to understand the causes of the seasonal ozone cycle shift across northern mid-latitudes and why the shift does not occur at all sites. These analyses should also be expanded to the NH polar and tropical regions as well as the SH.

## 7. Model-measurement comparison

While present-day in situ and satellite observations reveal much about the tropospheric ozone distribution and trends, at least for the past 50 years, much uncertainty remains regarding ozone mixing ratios and trends in remote areas such as the oceans or across sparsely sampled continental regions like Africa, the Middle East, South America and India. Additional uncertainty surrounds estimates of the global tropospheric ozone burden in pre-industrial times. In recent years chemistry-climate models (CCMs) have been employed to fill these gaps in our knowledge of tropospheric ozone (Horowitz, 2006; Stevenson et al., 2006; Lamarque et al., 2010; Stevenson et al., 2013; Young et al., 2013). The current generation of CCMs has been evaluated by the Atmospheric Chemistry and Climate Model Intercomparison Project (ACCMIP) (Young et al., 2013). The 15-model ensemble performed well in terms of reproducing major features of tropospheric ozone's global distribution and seasonal cycle. However the models display a high degree of variability regarding the components of the tropospheric ozone budget and a range of biases when compared to observations. Compared to OMI/MLS TCO the ACCMIP ensemble mean tropospheric column ozone is biased low by only 1%, however individual model biases range from –16% to +13%. These differences are more pronounced when examined by latitude with the SH mid-latitudes, SH tropics, NH tropics and NH mid-latitudes biased by –14%, –7%, 3% and 14%, respectively. The models also differ in their estimates of tropospheric ozone budget terms with chemical production, chemical loss and deposition ranging from 3877–5989 Tg ozone $a^{-1}$, 3638–5089 Tg ozone $a^{-1}$, and 687–1350 Tg ozone $a^{-1}$, respectively. The inter-model variability regarding estimates of tropospheric ozone burden and budget terms raises the question of how the models vary in their simulation of observed ozone trends. The ozone trends at the more remote sites considered in this paper provide critical tests of the accuracy of CCM global tropospheric ozone.

Parrish et al. (2014) have presented a systematic method of comparing these measured trends with model results, and provide a detailed comparison of 3 CCMs with trends at northern mid-latitudes. The models qualitatively reproduced many features of the measurements, but there were also substantial and consistent quantitative disagreements. In particular the models overestimated ozone mixing ratios (on average by 5 to 17 ppbv in the year 2000) and under-predicted the historical changes that have occurred in ozone mixing ratios. At the northern mid-latitude sites in Figure 1, observed trends average approximately 1% $yr^{-1}$ relative to the site's year 2000 mixing ratio (Parrish et al., 2014), while the modeled trends are roughly half that value.

The analysis of Parrish et al. (2014) focused on northern mid-latitudes and here we expand the scope of their methodology by comparing the same three CCMs to ozone monitoring sites beyond northern mid-latitudes (a description of each model can be found in the Appendix). Figure 14 shows modeled ozone trends for eight of the ten sites included in the right hand panel of Figure 1, displayed in the same format as the measurement figure. The qualitative agreement between the modeled and measured trends is striking. A particularly notable feature of Figure 1 is that the trends outside of northern mid-latitudes are much smaller than in that latitude band, which contains the large majority of anthropogenic emissions of ozone precursors.

The model results of Figure 14 are in significantly better quantitative agreement with the measurements than that reported for northern mid-latitudes by Parrish et al. (2014). The models still do overestimate ozone mixing ratios in the year 2000 on average, but by only 1 to 8 ppbv, and the correlation between the modeled and measured year 2000 ozone mixing ratios is quite high (0.80 to 0.88). The average (± 1 standard deviation) measured trend for the time period covered by the measurements (~1974 to the end of the available data) is 0.30 ± 0.29 % $yr^{-1}$ relative to the site's year 2000 mixing ratio, which is significantly positive, but only about one-third of the trend seen at northern mid-latitudes. The corresponding model average trends are between 0.04 and 0.22 % $yr^{-1}$ relative to the site's year 2000 mixing ratio, so the models agree that outside of northern mid-latitudes trends are small, but the models do underestimate the average trend, two of them to a statistically significant degree. Most notably, for the five SH sites, the models predict near zero average trends (–0.13 to +0.17 % $yr^{-1}$ relative to the site's year 2000 mixing ratio) while the measured trends indicate a small increase (average 0.28 % $yr^{-1}$ relative to the site's year 2000 mixing ratio).

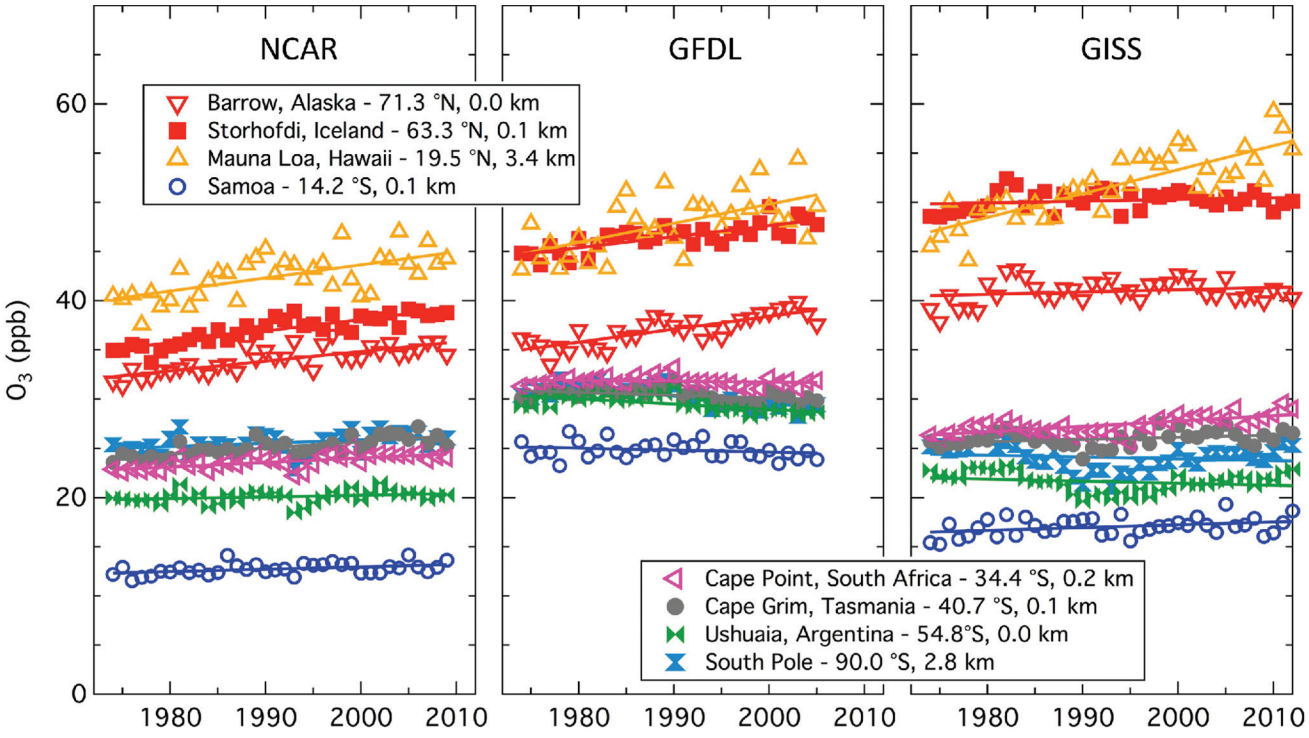


## 8. Conclusions

This literature review has provided an up-to-date characterization of tropospheric ozone distribution and trends based on studies published in the peer-reviewed scientific literature through 2014, with some new analysis of established datasets. The main conclusions are summarized as follows:

1) Based on modern studies that revisited late 19th century ozone observations, we have very limited confidence in the quantitative values of ozone measurements made with the Schönbein method and later converted to units of ppbv. Qualitatively however, Schönbein measurements are fairly consistent in revealing that 19th century seasonal ozone most often peaked in spring, followed by winter, with some spring peaks continuing into early summer. The only reliable quantitative ozone measurements from the late 19th century were made at Montsouris near Paris where ozone averaged 11 ± 2 ppbv from 1876 to 1910.
2) Observations indicate that tropospheric ozone increased globally during the 20th century. The longest quantitative ozone records are in Europe which indicate that ozone doubled there between the 1950s and 2000. From 1950–1979 until 2000–2010 all available NH monitoring sites indicate increasing ozone, with 11 of 13 sites having statistically significant trends of 1–5 ppbv decade$^{-1}$, corresponding to >100% ozone increases since the 1950s, and 9–55% ozone increases since the 1970s. In the SH only 6 sites are available, all indicating increasing ozone with 3 having statistically significant trends of 2 ppbv decade$^{-1}$. Ozone monitoring in the free troposphere since the 1970s is even more limited than at the surface. Significant positive trends since 1971 have been observed using ozonesondes above Western Europe, Japan and coastal Antarctica (rates of increase range from 1–3 ppbv decade$^{-1}$), but not at all levels. In addition, aircraft have measured significant upper tropospheric trends in one or more seasons above the northeastern USA, the North Atlantic Ocean, Europe, the Middle East, northern India, southern China and Japan. Notably, no site or region has shown a significant negative ozone trend in the free troposphere since the 1970s. From 1990 until 2010, surface ozone trends have varied by region. Western Europe showed increasing ozone in the 1990s followed by a leveling off, or decrease since 2000. In the eastern US surface ozone has decreased strongly in summer, is largely unchanged in spring, and has increased in winter, while ozone increases in the western US are strongest in spring. Surface ozone in East Asia is generally increasing.
3) The OMI/MLS tropospheric column ozone climatology shows that the NH experiences peak ozone values during boreal summer at mid-latitudes. The SH peak occurs in austral spring in the tropics and subtropics between South America and Africa and in a band centered at 25°S–30°S stretching from southern Africa eastward to Australia. On an annual basis NH average TCO exceeds the SH average by 4%, 12%, and 18% at low (0°–25°), mid- (25°–50°), and high (50°–60°) latitudes, respectively.

**Figure 14**

**A comparison between observed and modeled surface ozone trends.**

Model calculated surface ozone time series beginning in 1974 at eight of the rural sites outside of northern mid-latitudes shown in the right hand panel of Figure 1. The format of each panel corresponds to the third panel of Figure 1.

doi: 10.12952/journal.elementa.000029.f014

4) Monitoring at remote and rural surface sites around the globe shows that the lowest yearly average ozone mixing ratios are found in the MBL of the tropical South Pacific Ocean followed by the MBL of SH mid- and high latitudes. Ozone is greater in the NH MBL and increases over land and with elevation. In both the MBL and at high elevations in the NH, the greatest ozone mixing ratios at remote sites are found in western Japan, immediately downwind of East Asia where ozone precursor emissions have increased rapidly since 1980. A comparison of rural ozone measurements in heavily polluted regions in the USA, Europe and China shows that the greatest summertime ozone mixing ratios, based on the 50$^{th}$ and 95$^{th}$ percentiles of monthly daytime values, are found in northern China.
5) Qualitative ozone observations indicate that 19$^{th}$ century ozone concentrations most often peaked in spring, followed by winter, with some spring peaks continuing into early summer. By the end of the 20$^{th}$ century ozone in polluted regions had shifted to a summertime peak. However recent ozone precursor emission reductions are leading to reduced summertime ozone at northern mid-latitudes with some rural sites showing seasonal peak ozone shifting back to spring.
6) Comparison of output from three state-of-the-science chemistry-climate models to long-term ozone trends at remote surface sites shows that the models generally over-predict the ozone mixing ratios but under predict the rate of change. The disagreement is greatest for northern mid-latitudes.

While this review paper has addressed many aspects of tropospheric ozone it cannot cover all monitoring efforts and data analysis methods. Of the monitoring and analysis efforts not mentioned or elaborated upon above, we mention some of the most important ones here and point the interested reader towards the relevant references. In terms of measurements, the World Meteorological Organization's Global Atmosphere Watch program (http://www.wmo.int/pages/prog/arep/gaw/gaw_home_en.html) coordinates an extensive world-wide observation network. Over 400 sites conduct long term measurements of physical, chemical, meteorological and radiation parameters and make their quality-tested data freely available to the scientific community. Approximately 100 GAW stations measure surface ozone and the data are quality controlled for the detection of long term trends (Galbally and Schultz, 2013) and archived in the World Data Centre for Greenhouse Gases (http://ds.data.jma.go.jp/gmd/wdcgg).

In the free troposphere, the European In-service Aircraft for a Global Observing System (IAGOS) program (formerly known as MOZAIC and CARIBIC) has provided in situ observations of ozone, water vapor, carbon monoxide and other trace gases made from multiple commercial aircraft since 1994 (http://www.iagos.org). The program's goal is to instrument 10–20 aircraft belonging to airlines based around the world to produce a global tropospheric monitoring network. This extensive database has been utilized by over 200 peer-reviewed publications (see list at http://www.iagos.fr/web/rubrique4.html) and provides detailed ozone climatological and trend information across much of the NH (Thouret et al., 2006; Logan et al., 2012; Zbinden et al., 2013). In the coming years, expansion of the program will allow the calculation of ozone trends in the boundary layer and free troposphere at many more locations around the world (Saunois et al., 2012). Another monitoring program that is providing long-term information on free-tropospheric ozone is The Southern Hemisphere Additional Ozonesonde Network (SHADOZ, http://croc.gsfc.nasa.gov/shadoz) (Thompson et al., 2003, 2012). Established in 1998 the program coordinates a network of 11 ozonesonde stations, spread across the formerly data-sparse northern and southern tropics. Space-based monitoring of ozone will also be expanded by the year 2020 with the launch of new tropospheric ozone sounding instruments on low Earth orbiting satellites, and for the first time, geostationary satellites (Bowman, 2013).

Many of the ozone trend studies discussed in the main text examined not only the linear ozone trend but also variations in the rate of change in light of changing ozone precursor emissions. However recent studies are showing that interannual variability in atmospheric dynamics and long-term climate oscillations can also impact ozone trends on times-scales of 10–20 years. For example, variations in the quantity of ozone in the lowermost stratosphere or changing fluxes of the quantity of air transported from the stratosphere to the troposphere are associated with observed changes in surface and free tropospheric ozone (Ordóñez et al. 2007; Voulgarakis et al. 2011; Hess and Zbinden, 2013). El Niño–Southern Oscillation (ENSO) has also been linked to hemispheric and global scale tropospheric ozone interannual variability (Doherty et al., 2006; Koumoutsaris et al., 2008; Voulgarakis et al., 2010). Focusing on individual monitoring sites, ENSO and the Pacific –North American (PNA) pattern control the transport of ozone from East Asia to Mauna Loa, Hawaii producing very different ozone trends in spring and autumn (Lin et al., 2014), while the North Atlantic Oscillation modulates ozone at the high elevation site of Izaña in the subtropical North Atlantic Ocean (Cuevas et al., 2013).

The ozone trend studies referenced in this review are not the only papers available on this topic, but due to the different analysis techniques employed and/or varying time periods across which trends are calculated, difficulties arise when attempting to reconcile conflicting conclusions. For example, the few European time series referenced by this paper were selected because they are at least 20 years in length, long enough to show that ozone increased in the 1990s and levelled off in the 2000s. Other recent studies provide extremely informative and extensive trend analyses for dozens of ozone monitoring sites across Europe but the time series are either too short in length to assess any change in the ozone trend, or the

trends are reported in units other than ppbv $yr^{-1}$ (Wilson et al., 2012; Aggelis et al., 2013; Munir et al., 2013; Sicard et al., 2013).

In light of the problems associated with differing analysis techniques, and in recognition of the progress made by the International Workshops on Tropospheric Ozone Changes (Logan et al., 2010; Schultz et al., 2011), we support the organization of a community wide effort to produce a global Tropospheric Ozone Assessment Report (TOAR). Recently endorsed as an official activity of the International Global Atmospheric Chemistry (IGAC) Program (http://www.igacproject.org/TOAR) the goal of the report is to assess observational (in situ and satellite) and model studies in the peer-reviewed literature to provide a comprehensive overview of present-day global tropospheric ozone distribution and trends, uncertainties, and needs for future research and observations. In addition the report will provide updated summary statistics of surface and free tropospheric ozone observations and trends around the world, as well as ozone metrics designed for climate, human health and crop/ecosystem impact studies. Importantly, these ozone statistics and metrics will be produced using standard methods, units and time periods, providing the scientific community with a consistent and comprehensive quantification of this important trace gas.

# 9. Appendix

Following are the sources of the data used in the new analyses described in the main body of the manuscript, a brief discussion of trend uncertainties and descriptions of the chemistry-climate models discussed in Section 7.

### *Ozone data and emission inventories*

1) The OMI/MLS tropospheric column ozone climatology (Ziemke et al., 2011) was provided by co-author Jerald Ziemke, Morgan State University, Baltimore, and downloaded from: http://acd-ext.gsfc.nasa.gov/Data_services/cloud_slice/. The monthly data are averaged over the period October 2004 – December 2010 and reported at 5° × 5° horizontal resolution.
2) Monthly ozone statistics from the Miyun rural monitoring site in northern China were provided by co-author Yuxuan Wang, Center for Earth System Science, Tsinghua University, Beijing, China, and originally reported by Wang et al. (2010).
3) Hourly ozone data from Hohenpeissenberg for the years 1971–2008 were downloaded from the Global Atmosphere Watch (GAW) World Data Centre for Greenhouse Gases: http://ds.data.jma.go.jp/gmd/wdcgg. Data from 2009–2010 were provided by co-author Stefan Gilge.
4) Hourly ozone data at Ispra, Italy were collected by the Institute for Environment and Sustainability at the Joint Research Center-Ispra. The Ispra ozone monitor is a European Monitoring and Evaluation Programme (EMEP) station (station number IT0004) and therefore the data can be downloaded in units of μg $m^{-3}$ from the EBAS database (http://ebas.nilu.no). However, to directly compare Ispra to the other sites in this study, the data were required in units of ppbv as originally measured by the standard uv absorption technique employed at Ispra. These ppbv data were provided by co-author Niels R. Jensen.
5) Hourly ozone data from Gothic (Colorado), Beltsville (Maryland), Lassen Volcanic National Park (California) and Big Meadows, Shenandoah National Park (Virginia) were collected by The US EPA's Clean Air Status and Trends Network (CASTNET) and downloaded from: http://epa.gov/castnet/javaweb/index.html.
6) Hourly ozone data from Joshua Tree National Park were collected by the National Park Service Gaseous Pollutant Monitoring Program and downloaded from: http://ard-request.air-resource.com.
7) The Whiteface Mountain Summit ozone data set is the same data set analyzed by Cooper et al. (2012). The data were collected by the University at Albany-SUNY with instrumentation provided by the New York State Department of Environmental Conservation. The data set was provided by James J. Schwab, Atmospheric Sciences Research Center, University at Albany-SUNY. These data are also archived by the United States Environmental Protection Agency: http://www.epa.gov/ttn/airs/aqsdatamart/
8) The ozone data from Ushuaia, Argentina were provided by co-author Manuel Cupeiro. Hourly data can be downloaded from the Global Atmosphere Watch (GAW) World Data Centre for Greenhouse Gases: http://ds.data.jma.go.jp/gmd/wdcgg.
9) Yearly mean ozone values from Cape Point, South Africa were provided by Ernst Brunke, South African Weather Service, Stellenbosch. Hourly data can be downloaded from the Global Atmosphere Watch (GAW) World Data Centre for Greenhouse Gases: http://ds.data.jma.go.jp/gmd/wdcgg.
10) The hemispheric $NO_2$ emissions shown in Figure 4 are broken down by anthropogenic fuel combustion, biomass burning and lightning. Anthropogenic fuel $NO_x$ emissions (reported as $NO_2$) for the base year 2010 were obtained from the EDGAR HTAP_V2 global inventory: http://edgar.jrc.ec.europa.eu/htap_v2/index.php?SECURE=123. Biomass burning $NO_x$ emissions for the years 2005–2009 were obtained from the Global Fire Emissions Database (GFED3) (van der Werf et al., 2010). Global lightning $NO_2$ emissions were fixed at 5 Tg N (based on the best estimate of Schumann and Huntrieser [2007]) and distributed globally according to the LIS/OTD v2.2 gridded satellite lightning data (Christian et al.,

2003) produced by the NASA LIS/OTD Science Team (Principal Investigator, Dr. Hugh J. Christian, NASA/Marshall Space Flight Center) and available from the Global Hydrology Resource Center (http://ghrc.msfc.nasa.gov).

11) The global anthropogenic fuel $NO_x$ emissions shown in Figure 9 were taken from the EDGARv4.1 emission inventory for 2005 at $0.1^\circ \times 0.1^\circ$ resolution, provided by: European Commission, Joint Research Centre (JRC)/Netherlands Environmental Assessment Agency (PBL): Emission Database for Global Atmospheric Research (EDGAR), release version 4.1 http://edgar.jrc.ec.europa.eu, 2010.

### *Trend uncertainties*

The confidence limits of the trends included in Tables 1 and 2 and illustrated in Figure 2 provide guidance for assessing the veracity of the results; however, they have significant subtleties that must be appreciated. The confidence limits were determined from the least squares, linear regression fits to the time series of the respective data sets; they generally reflect the difficulty of discerning relatively small, long-term changes in seasonal or average ozone concentrations in the presence of large interannual variability arising from both atmospheric and measurement issues. Data sets with the least interannual variability give the smallest confidence limits and allow the detection of statistically significant long-term changes from the shortest possible records. Ozone concentrations in the atmosphere vary on all temporal scales from hourly or shorter through decadal and longer, with diurnal, synoptic and seasonal changes all being important. To determine long-term changes one must effectively average over all concentration changes occurring on time scales shorter than seasonal or annual. Hence, continuous hourly data records are ideal, since they can provide averages at any needed temporal resolution, but they are generally limited to surface observations. A regular program of ozonesonde or aircraft measurements can provide seasonal or annual averages, but they must be relatively frequent to effectively average over synoptic scale variability; Saunois et al., (2012) investigate the required frequency. Such a program must also consider time of day of measurements to avoid unwanted contributions to ozone variability from repetitive diurnal changes. Since sonde launches and aircraft flights are usually conducted only a few times per month at a given site, it is likely that some variability arising from synoptic changes remains in most such data records. A separate issue is experimental error. The most precise and accurate measurements will certainly provide the smallest confidence limits, and thus the most accurate determination of long-term changes. Random errors in the measurements at each temporal scale can contribute to that contribution to ozone variability. Systematic errors in the measurements, such as long-term drift in instrument calibration or changes in measurement procedures, are a potentially confounding factor that is not addressed by the confidence limits derived from the fitting procedures, since those procedures assume that all variability is random about a long term trend. Rigorous quality control procedures, such as have been implemented in many of the measurement networks whose data are discussed here, can minimize such errors. One indication of the strong statistical significance of the long-term changes discussed in this work is the spatial coherence of trends derived from different data sets collected in the same region (cf., Figures 1 and 2).

### *Chemistry-climate models*

The three models used in this study have the exact same configuration as the versions used in the recent northern mid-latitude analysis by Parrish et al. (2014). Due to the similarity in model configuration, data analysis techniques and contributing authors, the model descriptions below closely resemble the text in Parrish et al. (2014).

1) The global three-dimensional National Center for Atmospheric Research (NCAR) Community Coupled Chemistry-Climate Model (CAM-chem) includes interactive chemistry to calculate distributions of gases and aerosols in the troposphere and the lower to mid-stratosphere, from the surface to approximately 40 km (Lamarque et al., 2012). The standard model configuration includes a horizontal resolution of 1.9° (latitude) by 2.5° (longitude) and 26 hybrid levels up to 3.5 hPa, with a time-step of 30 minutes. Higher horizontal and vertical resolutions are available as well.

   In order to simulate the evolution of the atmospheric composition over the model vertical range, the chemical mechanism used in this study is formulated to represent both tropospheric and stratospheric chemistry as initially described by Lamarque et al. (2008). The model simulates the chemistry and transport of 117 gas species plus BC, OC, $SO_4$, $NO_3$, SOA, dust and sea salt. Extensive comparisons with observations (satellite, aircraft and ground-based) are discussed in Lamarque et al. (2012). In addition, CAM-chem has participated in a variety of model intercomparisons, e.g., The Atmospheric Chemistry and Climate Model Intercomparison Project (ACCMIP) (Lamarque et al., 2013).

   The comparison described in Section 7 uses the transient climate simulation results for 1951–2009, as described by Lamarque et al. (2013). Natural emissions include: interactive lightning $NO_x$, based on the model's convection and scaled to produce 3–5 TgN; constant pre-industrial soil $NO_x$ emissions; constant present-day biogenic isoprene, biogenic and oceanic CO, other VOCs and DMS; climate-sensitive dust, sea salt. Anthropogenic emissions are from the CMIP5 1850–2100 emissions database. Concentrations

of long-lived chemical species and greenhouse gases such as methane were prescribed, based on the observed historical record (1850–2005). Stratospheric ozone is produced by full stratospheric chemistry.

2) The Geophysical Fluid Dynamics Laboratory Coupled Model (GFDL-CM3) is a coupled atmosphere-ocean-land-ice model (Donner et al., 2011; Griffies et al., 2011) that simulates climate physics and tropospheric and stratospheric chemistry interactively over the full model domain (Austin et al., 2013; Naik et al., 2013). The standard model configuration uses a finite-volume atmospheric dynamical core on a cubed-sphere with a horizontal grid varying from 163 km at the six corners of the cubed sphere to 231 km near the center of each face, a resolution denoted as C48. Model results are interpolated to 2° latitude × 2.5° longitude grid. The vertical coordinate includes 48 hybrid pressure levels ranging in thickness from 70 m at the surface to 1–1.5 km in the upper troposphere to 2–3 km in most of the stratosphere, with a top level at 0.01 hPa (~86 km).

   CM3 simulates the atmospheric distributions of 97 chemical species interacting via 236 reactions throughout the model domain. Stratospheric and tropospheric chemistry are simulated seamlessly by combining the stratospheric chemistry formulation of Austin and Wilson (2010) and the tropospheric chemistry mechanism of Horowitz et al. (2003; 2007). Naik et al. (2013) and Austin et al. (2013) provide detailed descriptions and evaluations of the model's tropospheric and stratospheric chemistry, respectively. Long timescale coupled transient simulations of CM3 were performed for a range of experiments in support of the IPCC Fifth Assessment Report. Here, we employ results from one member of the 5-member ensemble historical (1860–2005) simulations (John et al., 2012; Austin et al., 2013; Eyring et al., 2013).

   The comparison described in Section 7 is based on model results for the period 1950 to 2005. The runs were forced with time-varying spatially-distributed anthropogenic and biomass burning emissions (Lamarque et al., 2010), globally uniform concentrations of greenhouse gases, including $CH_4$, carbon dioxide, nitrous oxide and halocarbons (Meinshausen et al., 2011), volcanic aerosols (Dentener et al., 2006), solar fluxes (Kopp et al., 2005), and land-use (Hurtt et al., 2011). Natural emissions of ozone precursors, except lightning $NO_x$, were held fixed at 2000 levels. Lightning $NO_x$ emissions were calculated interactively as a function of sub-grid convection in the model, and therefore varied in time.

3) The Goddard Institute for Space Studies Climate Model (GISS-E2-R) was run at 2° latitude by 2.5° longitude resolution, with increased effective resolution for tracers by carrying higher-order moments at each grid box (Shindell et al., 2013). The configuration used had 40 vertical hybrid sigma layers from the surface to 0.1 hPa (80 km). ACCMIP diagnostics for GISS-E2-R were saved from the GISS-E2-R CMIP5 transient climate simulations as those included fully interactive chemistry and aerosols. Those simulations were spun up for more than 1000 years, after which an ensemble of five simulations was performed for 1850–2012.

   The gas phase chemistry scheme included both tropospheric and stratospheric chemistry, with 156 chemical reactions among 51 species. Five of these reactions are heterogeneous, taking place on one, two or all three of the solid or liquid components included in the model: polar stratospheric clouds, sulfate dust aerosols. The model includes multiple aerosol components: sulfate, nitrate, carbonaceous (black and organic, both primary and secondary for the latter), mineral dust and sea-salt. Photolysis rates for 28 reactions are calculated, 26 of which use the Fast-J2 scheme (Bian and Prather, 2002) with parameterizations for two additional reactions that are important only at very high altitudes. Note that the model includes a reaction pathway for $HO_2$ + NO to yield $HNO_3$ (Butkovskaya et al., 2007). Detailed evaluation of the chemistry in this model has been documented previously (Shindell et al., 2013). Dry deposition is calculated using a resistance-in-series model coupled to a global, seasonally varying vegetation dataset. Wet deposition depends upon transport within convective plumes, scavenging within and below updrafts, rainout within both convective and large-scale clouds, washout below precipitating regions, evaporation of falling precipitation, and both detrainment and evaporation from convective plumes.

   The comparison described in Section 7 is based on model results for the period 1931 to 2012. Natural emissions in 2000 are $NO_x$ from lightning (7.3 Tg N $yr^{-1}$), and isoprene (536 Tg $yr^{-1}$). These emissions vary with climate. Natural emissions of $NO_x$ from soils are prescribed at fixed values (2.7 Tg N $yr^{-1}$), as are emissions of biogenic alkenes (16 Tg C $yr^{-1}$), paraffins (14 Tg C $yr^{-1}$) and terpenes (192 Tg $yr^{-1}$). The long-lived gases methane, nitrous oxide and CFCs are not emitted directly, but instead their concentrations are prescribed at the surface according to observations. Anthropogenic emissions are from the CMIP5 1850–2100 emissions database. Further detail on the model and emissions can be found in (Shindell et al., 2013).

## References

Aggelis D, Zanis P, Zerefos CS, Bais AF, Nastos PT. 2013. Mapping of Surface Ozone Seasonality and Trends Across Europe During 1997–2006 Through Kriging Interpolation to Observational Data. *Water Air Soil Pollut* **224**: 1501.

Anfossi D, Sandroni S, Viarengo S. 1991. Tropospheric ozone in the nineteenth century: The Moncalieri series. *J. Geophys. Res* **96**: 17,349–17,352.

Austin J, Wilson RJ. 2010. Sensitivity of polar ozone to sea surface temperatures and halogen amounts. *J. Geophys. Res* **115**: D18303. doi:10.1029/2009JD013292

Austin J, Horowitz LW, Schwarzkopf MD, Wilson RJ, Levy II H. 2013. Stratospheric ozone and temperature simulated from the preindustrial era to the present day. *J. of Climate* **26**: 3528–3543. doi:10.1175/JCLI-D-12-00162.1

Balashov NV, Thompson AM, Piketh S, Langerman K. 2014. Surface ozone variability and trends over the South African Highveld from 1990 to 2007. *J. Geophys. Res* **119**. doi:10.1002/2013JD02055

Beig G, Singh V. 2007. Trends in tropical tropospheric column ozone from satellite data and MOZART model. *Geophys. Res. Lett* **34**: L17801.

Bian H, Prather M. 2002. Fast-J2: Accurate simulations of photolysis in global climate models. *J. Atmos. Chem* **41**: 281–296.

Blunden J, Arndt DS, eds. 2013. State of the Climate in 2012. *Bull. Amer. Meteor. Soc* **94**(8): S1–S238.

Bojkov RD. 1986. Surface ozone during the second half of the nineteenth century. *J. Clim. Appl. Meteor* **25**: 343–352.

Bowman KW. 2013. Toward the next generation of air quality monitoring: Ozone. *Atmos.Environ* **80**: 571–583.

Butkovskaya N, Kukui A, Le Bras G. 2007. $HNO_3$ Forming Channel of the $HO_2$ + NO Reaction as a Function of Pressure and Temperature in the Ranges of 72–600 Torr and 223–323 K. *J. Phys. Chem. A* **111**: 9047–9053.

Butler TJ, Vermeylen FM, Rury M, Likens GE, Lee B, et al. 2011. Response of ozone and nitrate to stationary source $NO_x$ emission reductions in the eastern USA. *Atmos. Environ* **45**: 1084–1094.

Cartalis C, Varotsos C. 1994. Surface ozone in Athens, Greece, at the beginning and at the end of the Twentieth Century. *Atmos. Environ* **28**: 3–8.

Chameides W, Walker JCG. 1973. A photochemical theory of tropospheric ozone. *J. Geophys. Res* **78**(36): 8751–8760. doi:10.1029/JC078i036p08751

Christian HJ, Blakeslee RJ, Boccippio DJ, Boeck WL, Buechler DE, et al. 2003. Global frequency and distribution of lightning as observed from space by the Optical Transient Detector *J. Geophys. Res* **108**(D1): 4005. doi:10.1029/2002JD002347.

Cooper OR, Oltmans SJ, Johnson BJ, Brioude J, Angevine W, et al. 2011. Measurement of western U.S. baseline ozone from the surface to the tropopause and assessment of downwind impact regions. *J. Geophys. Res* **116**:D00V03. doi:10.1029/2011JD016095

Cooper OR, Gao R-S, Tarasick D, Leblanc T, Sweeney C. 2012. Long-term ozone trends at rural ozone monitoring sites across the United States, 1990–2010. *J. Geophys. Res* **117**: D22307. doi:10.1029/2012JD018261

Cooper O, Ziemke J. 2013. [Global Climate] Tropospheric Ozone, in "State of the Climate in 2012", *Bull. Amer. Meteor. Soc* **94**(8): S38–S39.

Cristofanelli P, Scheel H-E, Steinbacher M, Saliba M, Azzopardi F, et al. 2014. Long-term surface ozone variability at the Mt. Cimone WMO/GAW Global Station (2165 m a.s.l., Italy). *Atmos. Chem. Phys. Disc* **16**: EGU2014–6609.

Crutzen PJ. 1974. Photochemical reactions initiated by and influencing ozone in the unpolluted troposphere. *Tellus* **26**: 47–57.

Cuevas E, González Y, Rodríguez S, Guerra JC, Gómez-Peláez AJ, et al. 2013. Assessment of atmospheric processes driving ozone variations in the subtropical North Atlantic free troposphere. *Atmos. Chem. Phys* **13**:1973–1998.

Danielsen EF. 1968. Stratospheric-tropospheric exchange based on radioactivity, ozone and potential vorticity. *J. Atmos. Sci* **25**: 502–518.

Dentener F., Kinne S, Bond T, Boucher O, Cofala J, et al. 2006. Emissions of primary aerosol and precursor gases in the years 2000 and 1750 prescribed datasets for AeroCom. *Atmos. Chem. Phys* **6**: 4,321–4,344.

Dentener F, Keating T, H Akimoto H, eds. 2011. *Hemispheric Transport of Air Pollution 2010: Part A: Ozone and Particulate Matter*. New York: UN. (Air Pollut. Stud, vol. 17).

Derwent RG, Hjellbrekke A-G. 2013. Air Pollution by Ozone Across Europe, in Viana M, ed., *Urban Air Quality in Europe*. Berlin Heidelberg: Springer. (The Handbook of Environmental Chemistry, vol. 26): pp. 55–74. doi:10.1007/698_2012_163

Derwent RG, Manning AJ, Simmonds PG, Spain TG, Doherty S. 2013. Analysis and interpretation of 25 years of ozone observations at the Mace Head Atmospheric Research Station on the Atlantic Ocean coast of Ireland from 1987 to 2012. *Atmos. Environ* **80**: 361–368.

Ding AJ, Wang T, Thouret V, Cammas J-P, Nédélec P. 2008. Tropospheric ozone climatology over Beijing: analysis of aircraft data from the MOZAIC program. *Atmos. Chem. Phys* **8**: 1–13.

Doherty RM, Stevenson DS, Johnson CE, Collins WJ, Sanderson MG. 2006. Tropospheric ozone and El Niño–Southern Oscillation: Influence of atmospheric dynamics, biomass burning emissions, and future climate change. *J. Geophys. Res* **111**: D19304. doi:10.1029/2005JD006849

Donner LJ, Wyman BL, Hemler RS, Horowitz LW, Ming Y, et al. 2011. The dynamical core, physical parameterizations, and basic simulation characteristics of the atmospheric component of the GFDL global coupled model CM3. *J. Climate* **24**: 3,484–3,519. doi:10.1175/2011JCLI3955

European Environment Agency. 2013. *Air quality in Europe – 2013 report*, EEA Report No. 9/2013. Luxembourg: Publications Office of the European Union. doi:10.2800/92843, http://www.eea.europa.eu/publications/air-quality-in-europe-2013.

Eyring V, Arblaster JM, Cionni I, Sedlácek J, Perlwitz J, et al. (2013), Long-term ozone changes and associated climate impacts in CMIP5 simulations. *J. Geophys. Res* **118**: 5029–5060. doi: 10.1002/jgrd.50316

Fabian P, Pruchniewicz PG. 1977. Meridional distribution of ozone in the troposphere and its seasonal variation. *J. Geophys. Res* **82**: 2063–2073.

Feister U, Warmbt WG. 1987. Long-term measurements of surface ozone in the German Democratic Republic. *J. Atmos. Chem* **5**: 1–21.

Frost GJ, McKeen SA, Trainer M, Ryerson TB, Neuman JA, et al. 2006. Effects of changing power plant NOx emissions on ozone in the eastern United States: Proof of concept. *J. Geophys. Res* **111**: D12306. doi:10.1029/2005JD006354

Galbally IE, Schultz MG. 2013. *Guidelines for Continuous Measurement of Ozone in the Troposphere, GAW Report No 209, Publication WMO-No. 1110*. Geneva: World Meteorological Organisation: 76pp.

Gilge S, Plass-Duelmer C, Fricke W, Kaiser A, Ries L, et al. 2010. Ozone, carbon monoxide and nitrogen oxides time series at four alpine GAW mountain stations in central Europe. *Atmos. Chem. Phys* **10**: 12295–12316. doi:10.5194/acp-10-12295-2010

Gilliland AB, Hogrefe C, Pinder RW, Godowitch JM, Foley KL, et al. 2008. Dynamic evaluation of regional air quality models: Assessing changes in $O_3$ stemming from changes in emissions and meteorology. *Atmos. Environ* **42**: 5110–5123.

Granier C, Bessagnet B, Bond T, D'Angiola A, van der Gon HD, et al.2011. Evolution of anthropogenic and biomass burning emissions of air pollutants at global and regional scales during the 1980–2010 period. *Climatic Change* **109**:163–190. doi:10.1007/s10584-011-0154-1

Griffies SM, Winton M, Donner LJ, Horowitz LW, Downes SM, et al. 2011. The GFDL CM3 coupled climate model: characteristics of the ocean and sea ice simulations. *J. Climate* **24**: 3520–3544. doi:http://dx.doi.org/10.1175/2011JCLI3964.1

Haagen-Smit AJ. 1952. Chemistry and physiology of Los Angeles smog. *Industrial & Engineering Chemistry* **44**: 1342.

Hartmann DL, Klein Tank AMG, Rusticucci M, Alexander L, Brönnimann S, et al. 2013. Observations: Atmosphere and Surface Supplementary Material, in Stocker TF, Qin D, Plattner G-K, Tignor M, Allen SK, eds., *Climate Change 2013: The Physical Science Basis. Contribution of Working Group I to the Fifth Assessment Report of the Intergovernmental Panel on Climate Change*. New York: Cambridge University Press. Available from www.climatechange2013.org and www.ipcc.ch.

He H, Stehr JW, Hains JC, Krask DJ, Doddridge BG, et al. 2013. Trends in emissions and concentrations of air pollutants in the lower troposphere in the Baltimore/Washington airshed from 1997 to 2011. *Atmos. Chem. Phys* **13**: 7859–7874.

Helmig D, Oltmans SJ, Carlson D, Lamarque J-F, Jones A, et al. 2007. A review of surface ozone in the polar regions. *Atmos. Environ* **41**: 5138–5161.

Hess PG, Zbinden R. 2013. Stratospheric impact on tropospheric ozone variability and trends: 1990–2009. *Atmos. Chem. Phys* **13**: 649–674.

Hogrefe C. Hao W, Zalewsky EE, Ku Y-J, Lynn B, et al. 2011. An analysis of long-term regional-scale ozone simulations over the Northeastern United States: variability and trends. *Atmos. Chem. Phys* **11**: 567–582.

Horowitz LW, Walters S, Mauzerall DL, Emmons LK, Rasch PJ, et al. 2003. A global simulation of tropospheric ozone and related tracers: Description and evaluation of MOZART, version 2. *J. Geophys. Res* **108**: 4784. doi:10.1029/2002JD002853, D24

Horowitz LW. 2006. Past, present, and future concentrations of tropospheric ozone and aerosols: Methodology, ozone evaluation, and sensitivity to aerosol wet removal. *J. Geophys. Res* **111**: D22211. doi:10.1029/2005JD006937

Horowitz LW, Fiore AM, Milly GP, Cohen RC, Perring A, et al. 2007. Observational constraints on the chemistry of isoprene nitrates over the eastern Unites States. *J. Geophys. Res* **112**: D12S08. doi:10.1029/2006JD007747

Hurtt GC, Chini LP, Frolking S, Betts RA, Feddema J, et al. 2011. Harmonization of land-use scenarios for the period 1500–2100: 600 years of global gridded annual land-use transitions, wood harvest, and resulting secondary lands. *Clim Change* **109**(1): 117–161.

IPCC (Intergovernmental Panel on Climate Change). 2013. *Working Group I contribution to the IPCC Fifth Assessment Report "Climate Change 2013: The Physical Science Basis", Final Draft Underlying Scientific-Technical Assessment*. Available at http://www.ipcc.ch.

John J, Fiore AM, Naik V, Horowitz LW, Dunne JP. 2012. Climate versus emission drivers of methane lifetime against loss by tropospheric OH from 1860–2100. *Atmos. Chem. Phys* **12**: 12021–12036. doi:10.5194/acp-12-12021-2012

Junge CE. 1962. Global ozone budget and exchange between stratosphere and troposphere *Tellus* **14**: 363–377.

Kim SW, Heckel A, McKeen SA, Frost GJ, Hsie E-Y, et al. 2006. Satellite-observed U.S. power plant $NO_x$ emission reductions and their impact on air quality. *Geophys. Res. Lett* **33**: L22812. doi: 10.1029/2006GL027749

Kopp G, Lawrence G, G. Rottman G. 2005. The Total Irradiance Monitor (TIM): Science results. *Sol. Phys*. **230**: 129–140.

Koumoutsaris S, Bey I, Generoso S, Thouret V. 2008. Influence of El Niño–Southern Oscillation on the interannual variability of tropospheric ozone in the northern midlatitudes. *J. Geophys. Res* **113**(D19): 301. doi: 10.1029/2007JD009753

Langford AO, Senff CJ, Alvarez RJ, Banta RM, R. Hardesty M. 2010. Long-range transport of ozone from the Los Angeles Basin: A case study. *Geophys. Res. Lett* **37**: L06807. doi:10.1029/2010GL042507

Lamarque J-F, Kinnison DE, Hess PG, Vitt F. 2008. Simulated lower stratospheric trends between 1970 and 2005: identifying the role of climate and composition changes. *J. Geophys. Res* **113**: D12301. doi:10.1029/2007JD009277

Lamarque J-F, Bond TC, Eyring V, Granier C, Heil A, et al. 2010. Historical (1850–2000) gridded anthropogenic and biomass burning emissions of reactive gases and aerosols: methodology and application. *Atmos. Chem. Phys* **10**: 7017–7039.

Lamarque JF, Emmons LK, Hess PG, Kinnison DE, Tilmes S, et al. 2012. CAM-chem: description and evaluation of interactive atmospheric chemistry in the Community Earth System Model, *Geosci. Model. Dev* **5**: 369–411.

Lamarque J-F, Shindell DT, Josse B, Young PJ, Cionni I, et al. 2013. The Atmospheric Chemistry and Climate Model Intercomparison Project (ACCMIP): overview and description of models, simulations and climate diagnostics. *Geosci. Model Dev* **6**: 179–206. doi:10.5194/gmd-6-179-2013

Lee H-J, Kim S-W, Brioude J, Cooper OR, Frost GJ, et al. 2013. Transport of $NO_x$ in East Asia identified by satellite and in-situ measurements and Lagrangian particle dispersion model simulations. *J. Geophys. Res*. in-press.

Lefohn AS, Shadwick DS, Feister U, Mohnen VA. 1992. Surface –level ozone: Climate change and evidence for trends. *J. Air Waste Manage. Assoc* **42**: 136–144.

Lefohn AS, Shadwick D, Oltmans SJ. 2010. Characterizing changes in surface ozone levels in metropolitan and rural areas in the United States for 1980–2008 and 1994–2008. *Atmos. Environ* **44**: 5199–5210.

Lelieveld J, van Aardenne J, Fischer H, de Reus M, Williams J, et al. 2004. Increasing ozone over the Atlantic Ocean. *Science* **304**: 1483–1487.

Levy H. 1972. Photochemistry of the lower troposphere. *Planetary and Space Science* **20**: 919–935.

Li HC, Chen KS, Huang CH, Wang HK. 2010. Meteorologically adjusted long-term trend of ground-level ozone concentrations in Kaohsiung County, southern Taiwan. *Atmos. Environ* **44**: 3605–3608.

Lin Y-K, Lin T-H, Chang S-C. 2010.The changes in different ozone metrics and their implications following precursor reductions over northern Taiwan from 1994 to 2007. *Environ. Monit. Assess* **169**: 143–157. doi: 10.1007/s10661-009-1158-4

Lin M, Horowitz LW, Oltmans SJ, Fiore AM, Fan S. 2014. Tropospheric ozone trends at Mauna Loa Observatory tied to decadal climate variability. *Nature Geoscience* **7**: 136–143. doi: 10.1038/ngeo2066

Linvill DE, Hooker WJ, Olson B. 1980. Ozone in Michigan's environment 1876–1880. *Monthly Weather Review* **108**: 1883–1891.

Lisac I, Vujnović V, Marki A. 2010. Ozone measurements in Zagreb, Croatia, at the end of 19th century compared to the present data. *Meteorologische Zeitschrift* **19**: 169–178.

Liu SC, Trainer M, Fehsenfeld FC, Parrish DD, Williams EJ, et al. 1987. Ozone production in the rural troposphere and the implications for regional and global ozone distributions. *J. Geophys. Res* **92**(D4): 4191–4207. doi:10.1029/JD092iD04p04191

Logan JA, Prather MJ, Wofsy SC, McElroy MB. 1981. Tropospheric chemistry: A global perspective. *J. Geophys. Res* **86**(C8): 7210–7254. doi:10.1029/JC086iC08p07210

Logan JA. 1999. An analysis of ozonesonde data for the troposphere: Recommendations for testing 3-D models and development of a gridded climatology for tropospheric ozone *J. Geophys. Res* **104**: 16,115–16,150.

Logan J, Schultz M, Oltmans S. 2010. Observing and understanding tropospheric ozone changes: Tropospheric Ozone Changes Workshop: Boulder, Colorado, 14–16 October, 2009. *EOS, Transactions American Geophysical Union* **91**: 119.

Logan JA, Staehelin J, Megretskaia IA, Cammas J-P, Thouret V, et al. 2012. Changes in ozone over Europe: Analysis of ozone measurements from sondes, regular aircraft (MOZAIC) and alpine surface sites, *J. Geophys. Res* **117**: D09301. doi:10.1029/2011JD016952

Marenco A, Gouget H, Nédélec P, Pagés J-P. 1994. Evidence of a long-term increase in tropospheric ozone from Pic du Midi series: consequences: positive radiative forcing. *J. Geophys. Res* **99**: 16,617–16,632.

Meinshausen M, Smith SJ, Calvin K, Daniel SJ, Kainuma MLT, et al. 2011. The RCP greenhouse gas concentrations and their extension from 1765 to 2300, *Clim. Change* **109**: 213–241. doi:10.1007/s10584-011-0156-z

Monks PS. 2000. A review of the observations and origins of the spring ozone maximum. *Atmos. Environ* **34**: 3545–3561.

Monks PS, Granier C, Fuzzi S, Stohl A, Williams M, et al. 2009. Atmospheric Composition Change – Global and Regional Air Quality *Atmos. Environ* **43**: 5268–5350.

Munir S, Chen H, Ropkins K. 2013. Quantifying temporal trends in ground level ozone concentration in the UK. *Sci. Total Environ* **458–460**: 217–227.

Naik V, Horowitz LW, Fiore AM, Ginoux P, Mao J, et al. 2013. Impact of preindustrial to present day changes in short-lived pollutant emissions on atmospheric composition and climate forcing. *J. Geophys. Res* **118**: 8086–8110. doi:10.1002/jgrd.50608

National Research Council. 1991. *Rethinking the Ozone Problem in Urban and Regional Air Pollution, Committee on Tropospheric Ozone Formation and Measurement*. Washington, DC: National Academy Press.

Nolle M, Ellul R, Ventura F, Güsten H. 2005. A study of historical surface ozone measurements (1884–1900) on the island of Gozo in the central Mediterranean. *Atmos. Environ* **39**: 5608–5618.

Ojha N, Naja M, Singh KP, Sarangi T, Kumar R, et al. 2012. Variabilities in ozone at a semi-urban site in the Indo-Gangetic Plain region: Association with the meteorology and regional processes. *J. Geophys. Res* **117**: D20301. doi:10.1029/2012JD017716

Oltmans SJ, Komhyr WD. 1976. Surface ozone in Antarctica. *J. Geophys. Res* **81**: 5359–5364.

Oltmans SJ, Johnson BK, Harris JM. 2012. Springtime boundary layer ozone depletion at Barrow, Alaska: Meteorological influence, year-to-year variation, and long-term change. *J. Geophys. Res* **117**: D00R18. doi: 10.1029/2011JD016889

Oltmans SJ, Lefohn AS, Shadwick D, Harris JM, Scheel HE, et al. 2013. Recent tropospheric ozone changes — A pattern dominated by slow or no growth. *Atmos. Environ* **67**: 331–351.

Ordóñez C, Brunner D, Staehelin J, Hadjinicolaou P, Pyle JA, et al. 2007. Strong influence of lowermost stratospheric ozone on lower tropospheric background ozone changes over Europe. *Geophys. Res. Lett* **34**: L07805. doi:10.1029/2006GL029113

Parrish DD, Law KS, Staehelin J, Derwent R, Cooper OR, et al. 2012. Long-term changes in lower tropospheric baseline ozone concentrations at northern mid-latitudes. *Atmos. Chem. Phys* **12**: 11485–11504. doi:10.5194/acp-12-11485-2012

Parrish DD, Law KS, Staehelin J, Derwent R, Cooper OR, et al. 2013. Lower tropospheric ozone at northern mid-latitudes: Changing seasonal cycle. *Geophys. Res. Lett* **40**: 1631–1636. doi:10.1002/grl.50303

Parrish DD, Lamarque J-F, Naik V, Horowitz L, Shindell DT, et al. 2014. Long-term changes in lower tropospheric baseline ozone concentrations: Comparing chemistry-climate models and observations at northern mid-latitudes *J. Geophys. Res* in-press.

Pavelin EG, Johnson CE, Rughooputh S, Toumi R. 1999. Evaluation of pre-industrial surface ozone measurements made using Schönbein's method. *Atmos. Environ* **33**: 919–929.

Pozzoli L, Janssens-Maenhout G, Diehl T, Bey I, Schultz MG, et al. 2011. Reanalysis of tropospheric sulfate aerosol and ozone for the period 1980–2005 using the aerosol-chemistry-climate model ECHAM5-HAMMOZ. *Atmos. Chem. and Phys* **11**: 9563–9594.

Rieder HE, Fiore AM, Polvani LM, Lamarque J-F, Fang Y. 2013. Changes in the frequency and return level of high ozone pollution events over the eastern United States following emission controls. *Environ. Res. Lett* **8**: 014012. doi:10.1088/1748-9326/8/1/014012

Rosenthal JS, Helvey RA, Battalino TE, Fisk C, Greiman PW. 2003. Ozone transport by mesoscale and diurnal wind circulations across southern California. *Atmos. Environ* **37**: 51–71. doi:10.1016/S1352-2310(03)00382-0

Sandroni S, Anfossi D, Viarengo S. 1992. Surface ozone levels at the end of the nineteenth century in South America. *J. Geophys. Res* **97**: 2535–2539.

Saunois M, Emmons L, Lamarque J-F, Tilmes S, Wespes C, et al. 2012. Impact of sampling frequency in the analysis of tropospheric ozone observations. *Atmos. Chem. Phys* **12**: 6757–6773. doi:10.5194/acp-12-6757-2012

Scheel HE, Areskoug H, Gieß H, Gomiscek B, Granby K, et al. 1997. On the spatial distribution and seasonal variation of lower-troposphere ozone over Europe. *J. Atmos. Chem* **28**: 11–28.

Schnadt Poberaj C, Staehelin J, Brunner D, Thouret V, De Backer H, et al. 2009. Long-term changes in UT/LS ozone between the late 1970s and the 1990s deduced from the GASP and MOZAIC aircraft programs and from ozonesondes. *Atmos. Chem. Phys* **9**: 5343–5369.

Schultz M, Thouret V, Tarasova O, Cammas J-P, Galbally I, et al. 2011. *Report on the second international workshop on tropospheric ozone changes*. IGAC News, Issue No. 45, October, 2011, Melamed M, ed. http://igacproject.org.

Schumann U, Huntrieser H. 2007. The global lightning-induced nitrogen oxides source. *Atmos. Chem. Phys* **7**: 3823–3907.

Shindell DT, Pechony O, Voulgarakis A, Faluvegi G, Nazarenko L, et al. 2013. Interactive ozone and methane chemistry in GISS-E2 historical and future climate simulations. *Atmos. Chem. Phys* **13**: 2653–2689.

Sicard P, De Marco A, Troussier F, Renou C, Vas N, et al. 2013. Decrease in surface ozone concentrations at Mediterranean remote sites and increase in the cities. *Atmos. Environ* **79**: 705–715.

Staehelin J, Thudium J, Buehler R, Volz-Thomas A, Graber W. 1994. Trends in surface ozone concentrations at Arosa (Switzerland). *Atmos. Environ* **28**: 75–87.

Staehelin J, Schnadt Poberaj C. 2008. Long-term tropospheric ozone trends: A critical review, in Bronnimann S, Luterbacher J, Ewen T, Diaz HF, Stolarsk RS, Neu U, eds., *Climate Variability and Extremes during the past 100 years*. Heidelberg: Springer: pp. 271–282. (Advances in Global Change Research, vol. 33). doi: 10.1007/978-1-4020-6766-2_18

Stevenson DS, Dentener FJ, Schultz MG, Ellingsen K, van Moije TPC, et al. 2006. Multimodel ensemble simulations of present-day and near-future tropospheric ozone. *J. Geophys. Res* **111**: D08301. doi: 10.1029/2005JD006338

Stevenson DS, Young PJ, Naik V, Lamarque J-F, Shindell DT, et al. 2013. Tropospheric ozone changes, radiative forcing and attribution to emissions in the Atmospheric Chemistry and Climate Model Intercomparison Project (ACCMIP). *Atmos. Chem. Phys* **13**: 3063–3085. doi:10.5194/acp-13-3063-2013

Stohl A, Bonasoni P, Cristofanelli P, Collins W, Feichter J, et al. 2003. Stratosphere-troposphere exchange: A review, and what we have learned from STACCATO. *J. Geophys. Res* **108**(D12): 8516. doi:10.1029/2002JD002490

Sullivan TJ, Peterson DL, Blanchard CL. 2001. *Assessment of Air Quality and Air Pollutant Impacts in Class I National Parks of California*. Report, 421 pp., Natl. Park Serv., Denver, Colo. Available at http://nature.nps.gov/air/Pubs/pdf/reviews/ca/CAreport.pdf.

Tang GY, Wang Y, Li X, Ji D, Hsu S, et al. 2012. Spatial-temporal variations in surface ozone in Northern China as observed during 2009–2010 and possible implications for future air quality control strategies. *Atmos. Chem. Phys* **12**: 2757–2776.

Tarasick DW, Fioletov VE, Wardle DI, Kerr JB, Davies J. 2005. Changes in the vertical distribution of ozone over Canada from ozonesondes: 1980–2001. *J. Geophys. Res* **110**: D02304. doi:10.1029/2004JD004643

Tarasova OA, Senik IA, Sosonkin MG, Cui J, Staehelin J, et al. 2009. Surface ozone at the Caucasian site Kislovodsk High Mountain Station and the Swiss Alpine site Jungfraujoch: data analysis and trends (1990–2006). *Atmos. Chem. Phys* **9**: 4157–4175.

The Royal Society. 2008. Ground-level Ozone in the 21st century: Future Trends, Impacts and Policy Implications. *Royal Society policy document 15/08, RS1276*. Available at http://royalsociety.org/Report_WF.aspx?pageid57924&terms5ground-level1ozone

Thompson AM, Witte JC, McPeters RD, Oltmans SJ, Schmidlin FJ, et al. 2003. Southern Hemisphere Additional Ozonesondes (SHADOZ) 1998–2000 tropical ozone climatology 1. Comparison with Total Ozone Mapping Spectrometer (TOMS) and ground-based measurements *J. Geophys. Res* **108**(D2): 8238. doi:10.1029/2001JD000967

Thompson AM, Miller SK, Tilmes S, Kollonige DW, Witte JC, et al. 2012. Southern Hemisphere Additional Ozonesondes (SHADOZ) ozone climatology (2005–2009): Tropospheric and tropical tropopause layer (TTL) profiles with comparisons to OMI-based ozone products. *J. Geophys. Res* **117**: D23301. doi:10.1029/2011JD016911

Thouret V, Cammas J-P, Sauvage B, Athier G, Zbinden R, et al. 2006. Tropopause referenced ozone climatology and inter-annual variability (1994–2003) from the MOZAIC programme. *Atmos. Chem. Phys* **6**: 1033–1051.

*US Environmental Protection Agency*. 2009. *The $NO_x$ Budget Trading Program: 2008 Environmental Results. Available at* http://www.epa.gov/airmarkets/progress/NBP_3/NBP_2008_Environmental_Results.pdf

van der Werf GR, Randerson JT, Giglio L, Collatz GJ, Mu M, et al. 2010. Global fire emissions and the contribution of deforestation, savanna, forest, agricultural, and peat fires (1997–2009). *Atmos. Chem. Phys* **10**: 11,707–11,735. doi:10.5194/acp-10-11707-2010

Van Dingenen R, Dentener FJ, Raes F, Krol MC, Emberson L, et al. 2009. The global impact of ozone on agricultural crop yields under current and future air quality legislation. *Atmos. Environ* **43**(3): 604–618.

Volz A, Kley D. 1988. Evaluation of the Montsouris series of ozone measurements made in the nineteenth century. *Nature* **332**: 240–242.

Voulgarakis A, Savage NH, Wild O, Braesicke P, Young PJ, et al. 2010. Interannual variability of tropospheric composition: the influence of changes in emissions, meteorology and clouds *Atmos. Chem. Phys* **10**: 2491–2506.

Voulgarakis A, Hadjinicolaou P, Pyle JA. 2011. Increases in global tropospheric ozone following an El Nino event: examining stratospheric ozone variability as a potential driver. *Atmos. Sci. Lett* **112**: 228–232.

Wang T, Wei XL, Ding AJ, Poon CN, Lam KS, et al. 2009. Increasing surface ozone concentrations in the background atmosphere of Southern China, 1994–2007. *Atmos. Chem. Phys* **9**: 6217–6227.

Wang Y, Hao J, McElroy MB, Munger JW, Ma H, et al. 2010. Year round measurements of O3 and CO at a rural site near Beijing: variations in their correlations. *Tellus* **62B**: 228–241.

Warmbt W. 1964. *Luftchemische Untersuchungen des bodennahen Ozons 1952–1964: Methoden und Ergebnisse*. Berlin: Akademie-Verlag: 95p. (Abhandlungen des Meteorologischen Dienstes der Deutschen Demokratischen Republick Nr 72 [Band X]).

Wexler H, Moreland WB, Weyant WS. 1960. A preliminary report on ozoneobservations at Little America, Antarctica. *Mon. Wea. Rev* **88**: 43–54.

Wilson RC, Fleming ZL, Monks PS, Clain G, Henne S, et al. 2012. Have primary emission reduction measures reduced ozone across Europe? An analysis of European rural background ozone trends 1996–2005. *Atmos. Chem. Phys* **12**: 437–454.

Wu S, Mickley LJ, Jacob DJ, Logan JA, Yantosca RM, et al. 2007. Why are there large differences between models in global budgets of tropospheric ozone? *J. Geophys. Res* **112**: D05302. doi:10.1029/2006JD007801

Young PJ, et al. (2013), Pre-industrial to end 21st century projections of tropospheric ozone from the Atmospheric Chemistry and Climate Model Intercomparison Project (ACCMIP). *Atmos. Chem. Phys* **13**: 2063–2090. doi:10.5194/acp-13-2063-2013

Zbinden RM, Thouret V, Ricaud P, Carminati F, Cammas J-P, et al. 2013. Climatology of pure Tropospheric profiles and column contents of ozone and carbon monoxide using MOZAIC in the mid-northern latitudes (24° N to 50° N) from 1994 to 2009. *Atmos. Chem. Phys* **13**: 12363–12388.

Zellner R, Gesellschaft Deutscher Chemiker 2011. *Chemie über den Wolken … und darunter*. Weinheim, Germany: Wiley-VCH Verlag GmbH & Co. ISBN 978-3-527-32651-8

Ziemke JR, Chandra S, Bhartia PK. 2005. A 25-year data record of atmospheric ozone in the Pacific from Total Ozone Mapping Spectrometer (TOMS) cloud slicing: Implications for ozone trends in the stratosphere and troposphere. *J. Geophys. Res* **110**: D15105. doi:10.1029/2004JD005687

Ziemke JR, Chandra S, Duncan BN, Froidevaux L, Bhartia PK, et al. 2006. Tropospheric ozone determined from Aura OMI and MLS: Evaluation of measurements and comparison with the Global Modeling Initiative's Chemical Transport Model. *J. Geophys. Res* **111**: D19303. doi:10.1029/2006JD007089

Ziemke JR, Chandra S, Labow GJ, Bhartia PK, Froidevaux, et al. 2011. A global climatology of tropospheric and stratospheric ozone derived from Aura OMI and MLS measurements. *Atmos. Chem. Phys* **11**: 9237–9251.

**Data accessibility statement**

No new measurements were made for this review article. All ozone datasets mentioned in the text were obtained from existing databases, peer-reviewed publications, public research institutions, or government agencies, as described in the Appendix.

**Competing interests**

The authors declare no competing interests.

**Contributions**

- Contributed to conception and design: ORC
- Contributed to acquisition of data: all authors except ORC
- Contributed to analysis and interpretation of data: all authors
- Drafted and/or revised the article: ORC and DDP drafted the article while all others helped with the revision
- Approved the submitted and revised versions for publication: all authors